

1                   **MODIS vegetation products as proxies of photosynthetic potential:**

2                   **A look across meteorological and biologic driven ecosystem productivity**

3   Natalia Restrepo-Coupe<sup>1</sup>, Alfredo Huete<sup>1</sup>, Kevin Davies<sup>1,7</sup>, James Cleverly<sup>2,8</sup>, Jason Beringer<sup>3</sup>, Derek  
4   Eamus<sup>2,8</sup>, Eva van Gorsel<sup>4</sup>, Lindsay B. Hutley<sup>5</sup>, Wayne S Meyer<sup>6</sup>

5   [1] {Plant Functional Biology and Climate Change Cluster, University of Technology Sydney, PO Box 123, Broadway,  
6   NSW, 2007, Australia}

7   [2] {School of Life Sciences, University of Technology Sydney, PO Box 123, Broadway, NSW, 2007, Australia}

8   [3] {School of Earth and Environment, The University of Western Australia, Crawley, WA, 6009, Australia}

9   [4] {CSIRO Oceans and Atmosphere, Forestry House, Building 002, Wilf Crane Crescent, Yarralumla, ACT 2601,  
10   Australia}

11   [5] {Research Institute for the Environment and Livelihoods, Charles Darwin University, Darwin, NT 0909, Australia}

12   [6] {Environment Institute, School of Biological Sciences, University of Adelaide, Adelaide, SA, 5005, Australia}

13   [7] {School of Geosciences, University of Sydney NSW 2006, Australia}

14   [8] {Australian SuperSite Network}

15   **Correspondence to:** N. Restrepo-Coupe (nataliacoupe@gmail.com) and A. Huete  
16   (alfredo.huete@uts.edu.au)

17   **Type of paper:** Primary Research Article

18   **Keywords:** OzFlux, Australia, seasonality, ecosystem productivity, cross-site, MODIS, eddy  
19   covariance

## Abstract

1  
2 A direct relationship between gross ecosystem productivity (*GEP*) estimated by the eddy covariance  
3 (EC) method and Moderate Resolution Imaging Spectroradiometer (MODIS) vegetation indices (VIs)  
4 has been observed in many temperate and tropical ecosystems. However, in Australian evergreen  
5 forests, and particularly sclerophyll and temperate woodlands, MODIS VIs do not capture seasonality  
6 of *GEP*. In this study, we re-evaluate the connection between satellite and flux tower data at four  
7 contrasting Australian ecosystems, through comparisons of *GEP* and four measures of photosynthetic  
8 potential, derived via parameterization of the light response curve: ecosystem light use efficiency  
9 (*LUE*), photosynthetic capacity (*Pc*), *GEP* at saturation (*GEP<sub>sat</sub>*), and quantum yield ( $\alpha$ ), with MODIS  
10 vegetation satellite products, including VIs, gross primary productivity (*GPP<sub>MOD</sub>*), leaf area index  
11 (*LAI<sub>MOD</sub>*), and fraction of photosynthetic active radiation (*fPAR<sub>MOD</sub>*). We found that satellite derived  
12 biophysical products constitute a measurement of ecosystem structure (e.g. leaf area index - quantity of  
13 leaves) and function (e.g. leaf level photosynthetic assimilation capacity - quality of leaves), rather than  
14 *GEP*. Our results show that in primarily meteorological-driven (e.g. photosynthetic active radiation, air  
15 temperature and/or precipitation) and relatively aseasonal ecosystems (e.g. evergreen wet sclerophyll  
16 forests), there were no statistically significant relationships between *GEP* and satellite derived  
17 measures of greenness. In contrast, for phenology-driven ecosystems (e.g. tropical savannas), changes  
18 in the vegetation status drove *GEP*, and tower-based measurements of photosynthetic activity were best  
19 represented by VIs. We observed the highest correlations between MODIS products and *GEP* in  
20 locations where key meteorological variables and vegetation phenology were synchronous (e.g. semi-  
21 arid *Acacia* woodlands) and low correlation at locations where they were asynchronous (e.g.  
22 Mediterranean ecosystems). Although, we found a statistical significant relationship between the  
23 seasonal measures of photosynthetic potential (*Pc* and *LUE*) and VIs, where each ecosystem aligns  
24 along a continuum, we emphasize here that knowledge of the conditions in which flux tower  
25 measurements and VIs or other remote sensing products converge greatly advances our understanding

1 of the mechanisms driving the carbon cycle (phenology and climate drivers) and provides an ecological  
2 basis for interpretation of satellite derived measures of greenness.

### 3 **1. Introduction**

4 Eddy flux towers constitute a powerful tool to measure and study carbon, energy and water fluxes.  
5 Even though the number of eddy covariance (EC) sites has been steadily increasing (Baldocchi, 2014;  
6 Baldocchi et al., 2001), instrumentation, personnel costs, and equipment maintenance limit the  
7 establishment of new sites. This is demonstrated by the distribution of flux towers around the world  
8 and in particular the under-representation of tropical and semi-arid locations in the southern hemisphere  
9 (Australia, Africa, and South America) (<http://fluxnet.ornl.gov/maps-graphics> and Beringer et al.  
10 (2007)). The first EC tower was established in 1990 at Harvard Forest (Wofsy et al., 1993) followed by  
11 five other sites in 1993 (Baldocchi, 2003). In Australia, only two locations, Howard Springs (AU-  
12 How; Hutley et al. (2000)) and Tumbarumba (AU-Tum; Leuning et al., (2005)), have a record that  
13 extends more than 10 years.

14 Many applications rely on large-scale, remotely sensed (RS) representations of vegetation dynamics  
15 (greenness) to: (1) up-scale water and carbon fluxes from the limited tower footprint (radius <10 km)  
16 representative of eddy covariance measurements, (2) scale fluxes in time and extend a longer time  
17 series from limited tower data, (3) fill gaps due to quality control in the flux measurements, (4) study  
18 continental phenology to be validated at flux tower sites, and (5) parameterise land surface (LSMs) and  
19 agricultural models to be tested at EC locations. Past studies have focused on the relationship between  
20 the Moderate Resolution Imaging Spectroradiometer (MODIS) VIs, such as the enhanced vegetation  
21 index (*EVI*), and tower based measurements of gross ecosystem productivity (*GEP*) (Gamon et al.,  
22 2013; Huete et al., 2008, 2006; Maeda et al., 2014; Sims et al., 2006; Wang et al., 2004). In this

1 studies, satellite derived vegetation indices (VIs) represented a community property of chlorophyll  
2 content, leaf area index (*LAI*), and fractional vegetation cover. A simple linear regression between  
3 seasonal (monthly or 16-day) *EVI* and *GEP* has previously provided a good coefficient of  
4 determination ( $R^2$ ) for different ecosystems:

$$5 \quad GEP = b_0 + b_1 \times EVI \quad (1)$$

6 where  $b_0$  and  $b_1$  are the fitted coefficients. Huete et al. (2006) reported an  $R^2$  of 0.5 for Eq. 1 in tropical  
7 forests and converted pastures over the Amazon basin, and an  $R^2$  of 0.74 in dry to humid tropical forest  
8 sites in Southeast Asia (Huete et al., 2008). Over the North Australian mesic and xeric tropical  
9 savannas,  $R^2$  ranged from 0.52 at a wooded grassland (Alice Springs, AU-ASM) to 0.89 in woodlands  
10 (Howard Springs, AU-How) (Ma et al., 2013).

11 Similar relationships to Eq. 1 have been explored using monthly maximal net ecosystem exchange  
12 ( $NEE_{max}$ ):

$$13 \quad NEE_{max} = b_0 + b_1 \times EVI \quad (2)$$

14 This regression showed an improved fit in forests ( $R^2=0.83$  for deciduous and  $R^2=0.72$  for coniferous  
15 forests) compared to the *GEP-EVI* model ( $R^2=0.81$  for deciduous and  $R^2=0.69$  for evergreen forests)  
16 (Olofsson et al., 2008).

17 Other approaches to link carbon fluxes to RS products include radiation-greenness (R-G) models,  
18 where both a meteorological driver, represented by the photosynthetic active radiation (*PAR*), and a

1 vegetation phenology driver, represented by *EVI* or by the normalized difference vegetation index  
2 (*NDVI*), are implicitly included in the model (Ma et al., 2014; Peng and Gitelson, 2012). By definition,  
3 the *GEP/PAR* ratio is commonly referred as ecosystem light use efficiency (*LUE*), where:

$$4 \quad LUE = b_0 + b_1 \times EVI \quad (3)$$

5 However, the *EVI versus LUE* relationship has shown lower  $R^2$  values (0.76) compared to the *EVI*  
6 *versus GEP* regression (0.92) for a group of North American ecosystems that included evergreen  
7 needleleaf and deciduous forests, grasslands and savannas (Sims et al., 2006). Hill et al. (2006) also  
8 reported an  $R^2$  of  $\sim 0.2$  for the *NDVI versus LUE* relationship for the Australian sclerophyll forest of  
9 Tumbarumba (AU-Tum); however, this result was not statistically significant ( $p > 0.05$ ). To better  
10 represent *GEP* at rainfall-driven semi-arid ecosystems, Sjöström et al. (2011) increased the level of  
11 complexity of the R-G model by scaling down observations of *PAR* using the evaporative fraction (*EF*)  
12 term from EC measurements (a proxy for water availability), thus *GEP* was calculated as:

$$13 \quad GEP = EVI \times PAR \times EF \quad (4)$$

14 where *EF* is the ratio between latent heat flux (*LE*) and the surface turbulent fluxes ( $H+LE$ ), and *H* is  
15 defined as the sensible heat flux,  $EF = LE / (H+LE)$ . The model increased the predictive power of the  
16 R-G model in some ecosystems; however, it was not applicable at regional scales due to its reliance  
17 upon supporting tower measurements.

18 Temperature-greenness models (T-G) use the MODIS Land Surface Temperature product (*LST*) and  
19 VIs to calculate *GEP* as in Sims et al. (2008). The T-G *GEP* model for nine North American temperate  
20 EC sites was calculated as:

1  $GEP = EVI_{scaled} \times LST_{scaled} \times m$  (5)

2 where  $m$  is a function of mean annual  $LST$  and plant functional type (different formulation provided for  
3 evergreen and deciduous vegetation),  $LST_{scaled}$  is the minimum of two equations ( $LST/30$ ) and ( $2.5 -$   
4  $(0.05 \times LST)$ ), and  $EVI_{scaled}$  is  $EVI - 0.10$ . A similar T-G model, used by Wu et al. (2011), showed high  
5 correlation at deciduous forests ( $R^2 = \sim 0.90$ ) and lower  $R^2$  values at non-forest areas ( $R^2 = 0.27$  to  $0.91$ )  
6 and evergreen forests ( $R^2 = 0.28$  to  $0.91$ ).

7 Other more complex derivations, including the C-Fix model (Veroustraete et al., 2002) and the MODIS  
8 Gross Primary Productivity product ( $GPP_{MOD}$ ), rely on biome specific relationships that include: (1)  
9 vegetation phenology represented by MODIS derived fraction of absorbed PAR that a plant canopy  
10 absorbs for photosynthesis and growth ( $fPAR_{MOD}$ ); and (2) air temperature ( $T_{air}$ ), water vapour pressure  
11 deficit ( $VPD$ ), and  $PAR$  as climate drivers (Running et al., 2000). When applied to Australian  
12 ecosystems, the  $GPP_{MOD}$  (collection 4) was able to estimate the amplitude of the  $GEP$  annual cycle in  
13 an temperate evergreen wet sclerophyll forest (*Eucalyptus* dominated), however, it was out-of-phase  
14 (Leuning et al., 2005). For a tropical savanna (AU-How),  $GPP_{MOD}$  (collection 5) overestimated dry  
15 season  $GEP$  (Kanniah et al., 2009). Even though,  $GPP_{MOD}$  (collection 4.8) at AU-How accurately  
16 represented seasonality in productivity; low estimates of  $PAR$  and other model input variables were  
17 compensated by abnormally high  $fPAR_{MOD}$  values (Kanniah et al., 2009). A clear indication of  
18 obtaining a good result for the wrong reasons.

19

20 Besides the difficulties inherent in determining  $GEP$  in diverse ecosystems, all of the complex models  
21 (e.g.  $GPP_{MOD}$  and T-G model) require in situ measurements of water fluxes,  $PAR$ , and/or biome  
22 classification information to calibrate or derive some variables and consequently, regression

1 coefficients do not necessarily extend to ecosystem types other than those for which the derivation was  
2 obtained. Our first objective was to revisit the *GEP versus EVI*, and *GEP versus GPP<sub>MOD</sub>* regressions  
3 at different sites to gain a better understanding of ecosystem behaviour rather, than simply to determine  
4 the “best performing model”. We look at particularly challenging land cover classes: seasonal wet-dry  
5 and xeric tropical savannas, Mediterranean environments characterized by hot and dry summers  
6 (Mallee), and temperate evergreen sclerophyll forests. The selected locations are part of the OzFlux  
7 eddy-covariance network and represent sites where previous studies have shown satellite derived *GEP*  
8 models to be unable to replicate *in situ* measurements.

9 Our second objective was to derive using the light response curve different ground-based measures of  
10 vegetation photosynthetic potential: quantum yield ( $\alpha$ ), photosynthetic capacity ( $P_c$ ), *GEP* at saturation  
11 light ( $GEP_{sat}$ ), and ecosystem light use efficiency ( $LUE$ ) in an attempt to separate the vegetation  
12 structure and function (phenology) from the climatic drivers of productivity. We explored the  
13 seasonality of the four measures of photosynthetic potential ( $\alpha$ ,  $P_c$ ,  $LUE$ ,  $GEP_{sat}$ ) and aimed to  
14 determine if *EVI* was able to replicate absolute value and their annual cycle rather than photosynthetic  
15 activity (*GEP*), based on linear regressions. Similarly, we included in our analysis other MODIS  
16 biophysical datasets ( $NDVI$ ,  $LAI_{MOD}$ , and  $fPAR_{MOD}$ ) in an effort to understand how to interpret different  
17 satellite measures of greenness and how these products can inform modellers and ecologists about  
18 vegetation phenology. In contrast to biome-specific classification approaches, we treated the  
19 relationship between greenness and photosynthetic potential to be a continuum and therefore, we  
20 explored multiple site regressions.

21 Our third objective was to combine satellite-derived meteorology (radiation, precipitation and  
22 temperature) and biological drivers (vegetation phenology) to determine site specific and multi-biome  
23 *GEP* values using multiple regression models. In this study, we evaluated the advantages of

1 introducing both types of variables; we explored if the regressions hold across biomes, and whether  
2 productivity processes are driven by phenology, light, water availability, and/or temperature; and we  
3 infer which of these variables govern the *GEP* seasonal cycle for each particular ecosystem. These  
4 results advance our understanding of driving mechanisms of the carbon cycle (climate, biological  
5 adaptation, or a combination of both), temporal and spatial scaling, and provide an ecological basis for  
6 the interpretation of satellite derived measures of greenness and phenology products.

## 7 **2. Methods**

### 8 **2.1. Study sites**

9 The OzFlux infrastructure network is operated by a collaborative research group and was set up to  
10 provide the Australian and global ecosystem modelling communities with CO<sub>2</sub> and H<sub>2</sub>O flux and  
11 meteorological data (Beringer et al., 2016). We selected four contrasting long-term eddy flux (EC)  
12 sites from the OzFlux network (Figure 1 and Table 1) for this study.

13 In northern Australia the Howard Springs (AU-How) eddy flux tower is located in the Black Jungle  
14 Conservation Reserve, an open woodland savanna dominated by an understory of annual grasses and  
15 two overstory tree species: *Eucalyptus miniata* and *Eucalyptus tentrodonata* (Hutley et al., 2011;  
16 Kanniah et al., 2011). In the middle of the continent, among the xeric tropical savannas, the Alice  
17 Springs Mulga site (AU-ASM) is located in a semi-arid Mulga woodland dominated by *Acacia aneura*  
18 and different annual and perennial grasses including Mitchell Grass (gen. *Astrebla*) and *Spinifex* (gen.  
19 *Triodia*) (Cleverly et al., 2013; Eamus et al., 2013). Classified as a Mediterranean environment and  
20 characterized by hot and dry summers, the Calperum-Chowilla flux tower (AU-Cpr), is located at the  
21 fringes of the River Murray floodplains, a Mallee site (multi-stemmed *Eucalyptus socialis* and *E.*  
22 *dumosa* open woodland) (Meyer et al., 2015). The evergreen Tumbarumba (AU-Tum) site is located in  
23 Bago State Forest, NSW and classified as temperate evergreen wet sclerophyll (hard-indigestible



1 leaves) forest. It is dominated by 40 m tall *Eucalyptus delegatensis* trees (Leuning et al., 2005; van  
2 Niel et al., 2012).

3 Fluxes at all towers were measured by the EC method with an open-path system. Simultaneously, an  
4 array of different sensors measured meteorological data including air temperature ( $T_{air}$ ), relative  
5 humidity ( $RH$ ), incoming and reflected short wave radiation ( $SW_{down}$  and  $SW_{up}$ ), and incoming and  
6 reflected long wave radiation ( $LW_{down}$  and  $LW_{up}$ ). Refer to each site references for complete information  
7 regarding ecosystem and measurement techniques.

## 8 **2.2. Eddy covariance data**

9 We used Level 3 OzFlux data that includes an initial OzFlux standard quality control (QA) (Isaac et al.,  
10 2016). All data were subject to the same quality assurance procedures and calculations, providing  
11 methodological consistency among sites and reducing the uncertainty of the calculated fluxes. We  
12 performed additional quality checks and removal of outliers, and data were corrected for low  
13 turbulence periods (see Section 2.2.1). Ecosystem respiration ( $R_{eco}$ ) and  $GEP$  were calculated from EC  
14 measurements of net ecosystem exchange ( $NEE$ ) as presented in Section 2.2.2. Finally, we derived  
15 different measures of ecosystem vegetation photosynthetic potential (Section 2.2.3).

### 16 **2.2.1. Eddy covariance and meteorological measurements**

17 Incoming and outgoing radiation, both shortwave ( $SW_{down}$  and  $SW_{up}$ ) and longwave ( $LW_{down}$  and  $LW_{up}$ ),  
18 were measured using a CNR1 Net Radiometer instrument (Campbell Scientific). All sensors were  
19 placed above the canopy at the same height or higher than the EC system. As there were no  
20 measurements of  $PAR$  radiation available at AU-ASM, AU-Tum and AU-Cpr, we assumed  $PAR = 2 \times$   
21  $SW$  (Papaioannou et al., 1993; Szeicz, 1974), where  $PAR$  is measured as flux of photons ( $\mu\text{mol m}^{-2} \text{s}^{-1}$ )  
22 and  $SW_{down}$  as heat flux density ( $\text{W m}^{-2}$ ). We understood this as an approximation because  $PAR$

1 radiation (0.4 -0.7 nm) is a spectral subset of  $SW_{down}$  (0.3 – 3 nm).

2 At AU-Tum, the  $NEE$  is calculated as the sum of the turbulent flux measured by eddy covariance ( $F_C$ )

3 plus changes in the amount of  $CO_2$  in the canopy air space (storage flux,  $S_{co2}$ ), where  $NEE = F_C + S_{co2}$ .

4 At all other sites, given the sparse vegetation cover and the smaller control volume over the vegetation

5 which is lower in height,  $F_C$  is assumed to be representative of  $NEE$ .

6 Hourly fluxes measured during rainy periods, when the sonic anemometer and the open path infrared

7 gas analyser (IRGA) do not function correctly, were identified and removed from the time series. We

8 also removed isolated observations (between missing values). We identified any residual spikes from

9 the hourly  $NEE$  data using the method proposed by Papale et al. (2006) and modified by Barr et al.

10 (2009). For each hour ( $i$ ), the measure of change in  $NEE$  ( $d_i$ ) from the previous ( $i-1$ ) and next ( $i+1$ )

11 time step is calculated as:

$$12 \quad d_i = (NEE_i - NEE_{i-1}) - (NEE_{i+1} - NEE_i) \quad (6)$$

13 A spike is identified if the change is outside a given range:

$$14 \quad Md - \left( \frac{z \times \text{median}|d_i - Md|}{0.6745} \right) < d_i > Md + \left( \frac{z \times \text{median}|d_i - Md|}{0.6745} \right) \quad (7)$$

15 where  $Md$  is the median of the differences ( $d_i$ ),  $\pm 0.6745$  are the quartiles for a standard normal

16 distribution, and the constant  $z$  was conservatively set to 5 (Restrepo-Coupe et al., 2013).

### 2.2.2. Ecosystem respiration ( $R_{eco}$ ) and gross ecosystem productivity ( $GEP$ )

Night-time hourly  $NEE$  values were corrected for periods of low turbulent mixing by removing them from the time series data. Low turbulent missing periods were determined when friction velocity ( $u^*$  in  $m\ s^{-1}$ ) was below a threshold value ( $u^*_{thresh}$ ) as described in Restrepo-Coupe et al. (2013). Table 1 presents site-specific  $u^*_{thresh}$  values and the corresponding upper and lower confidence bounds.

Night-time  $NEE$  was assumed to be representative of ecosystem respiration ( $R_{eco}$ ) and it was calculated by fitting  $R_{eco}$  to a second-order Fourier regression based on the day of the year ( $DOY$ ) as in Richardson and Hollinger (2005):

$$R_{eco} = fo + s_1 \sin(Dpi) + c_1 \cos(Dpi) + s_2 \sin(2 Dpi) + c_2 \cos(2 Dpi) + e \quad (8)$$

where,  $fo$ ,  $e$ ,  $s_1$ ,  $c_1$ ,  $s_2$ , and  $c_2$  are the fitted coefficients and  $Dpi = DOY \times 360/365$  in radians. This method calculates  $R_{eco}$  with minimal use of environmental covariates. In order to determine the consistency of the Fourier regression method and the low friction velocity ( $u^*$ ) filter on the modelled  $R_{eco}$  (directly dependent of night-time  $NEE$  values), we compared the results presented here to  $R_{eco}$  values based on the intercept of the relation (rectangular hyperbola) between  $NEE$  and  $SW_{down}$  (for no incoming radiation,  $SW_{down} = 0$ ) (Suyker and Verma, 2001) (Supplement Figure 1).

Gross ecosystem exchange ( $GEE$ ) was calculated as the difference between  $NEE$  and  $R_{eco}$  ( $GEE = NEE + R_{eco}$ ). We defined gross ecosystem productivity ( $GEP$ ) as negative  $GEE$  (positive values of  $GEP$  flux indicate carbon uptake). For a 16-day moving window, we fitted two rectangular hyperbolas on the relationship between incoming  $PAR$  and  $GEP$  observations (separating morning and afternoon values) as in Johnson and Goody (2011) and based on the Michaelis and Menten formulation (1913):

1 
$$GEP = \frac{\alpha \times GEP_{sat} \times PAR}{GEP_{sat} + (\alpha \times PAR)}$$
 (9)

2 where  $\alpha$  is the ecosystem apparent quantum yield for CO<sub>2</sub> uptake (the initial slope), and  $GEP_{sat}$  is  $GEP$   
3 at saturating light (the asymptote of the regression) (Falge et al., 2001) (Figure 2). Our intention was to  
4 compare 16-day MODIS data to observations rather than to model a complete time series. We  
5 therefore, filled infrequent  $GEP$  missing values only if in a 16 day period there were 30 hours of  
6 measurements.

7 We obtained similar seasonal patterns and good agreement using different methods for calculating  $GEP$   
8 and  $R_{eco}$  (Supplement Fig. 1). We observed no statistically significant seasonal differences between  
9 calculating  $R_{eco}$  as the intercept of the light response curve (Falge et al., 2001) and  $NEE$  not subject to  
10  $u^{*}_{thresh}$  correction ( $R_{eco\ LRC}$ ), to calculating  $R_{eco}$  using the Fourier regression method (slope  $\sim 0.87$  and  
11  $R^2=0.94$  linear regression between  $R_{eco\ LRC}$  and  $R_{eco}$ ). This comparison increased our confidence in using  
12 either method to derive  $GEP$  and  $R_{eco}$  fluxes from the EC data, the absolute values and the seasonality  
13 here presented.

14  $GEP$  and  $GPP$  (true photosynthesis minus photorespiration (Wohlfahrt and Gu, 2015)) have been used  
15 interchangeably in the literature. However,  $GPP$  in this study was distinguished from  $GEP$ , thus as  
16  $GEP$  does not include CO<sub>2</sub> recycling at leaf-level (i.e. re-assimilation of dark respiration) or below the  
17 plane of the EC system (i.e. within canopy volume) (Stoy et al., 2006). Differences may be important  
18 when comparing tower-flux observations of  $GEP$  to the MODIS  $GPP$  (see next section).

### 2.2.3. Four measures of ecosystem photosynthetic potential: $\alpha$ , $LUE$ , $GEP_{sat}$ , and $Pc$

Measures of photosynthetic potential constitute an attempt to separate the inherent vegetation properties that contribute to photosynthetic activity ( $GEP$ ) from the effects of the meteorological influences on productivity using the parametrization of the 16-day light response equation. The variables  $\alpha$ ,  $LUE$ ,  $GEP_{sat}$ , and  $Pc$  were intended to represent an ecosystem property, a descriptor of the vegetation phenology similar to leaf area index ( $LAI$ ) or above ground biomass ( $AGB$ ). We calculated 16-day mean  $\alpha$  and  $GEP_{sat}$ , which are the two coefficients that define the  $GEP$  versus  $PAR$  rectangular hyperbola (Eq. 5) as a measure of the vegetation structure and function (Figure 2). Both  $\alpha$  ( $\mu\text{mol CO}_2 \text{ mmol}^{-1}$ ) and  $GEP_{sat}$  ( $\mu\text{mol CO}_2 \text{ m}^{-2} \text{ s}^{-1}$ ) values are known to vary with vegetation type, temperature, water availability and  $\text{CO}_2$  concentration. The  $GEP_{sat}$  represents the ecosystem response at saturating levels of  $PAR$ , usually constrained by high vapour pressure deficit ( $VPD$ ), air temperature ( $T_{air}$ ), water availability, and foliar N, among other variables (Collatz et al., 1991; Ehleringer et al., 1997; Tezara et al., 1999). By contrast,  $\alpha$  is measured at low light levels, when diffuse radiation is high (cloudy periods, sunset and sunrise). Ecosystem light use efficiency ( $LUE$ ) was defined as the mean daily  $GEP/PAR$  ratio. Therefore,  $LUE$  includes the effect of day length, the radiation environment (diffuse versus direct), water availability and other physical factors.

We used the relationships between tower measured  $GEP$ ,  $PAR$ , and  $VPD$  to characterize the photosynthetic capacity of the ecosystem ( $Pc$ ). Where  $Pc$  was defined as the average  $GEP$  for incoming radiation at light levels that are non-saturating -values between the annual daytime mean  $PAR \pm 100 \mu\text{mol m}^{-2} \text{ s}^{-1}$  (940, 1045, 788 and 843  $\mu\text{mol m}^{-2} \text{ s}^{-1}$  at AU-How, AU-ASM, AU-Tum and AU-Cpr, respectively) and  $VPD$  ranges between annual daytime mean  $\pm 2$  standard deviations (Figure 2) (Hutyra et al., 2007; Restrepo-Coupe et al., 2013).  $Pc$  was interpreted as a measure of the built capacity without taking into account the day-to-day changes in available light, photoperiod, and extreme  $VPD$  and  $PAR$  values. The derivation of  $Pc$  did not take into account other variables such as  $T_{air}$  or soil water

1 content.

## 2 2.3. Remote sensing data

### 3 2.3.1. Moderate Resolution Imaging Spectroradiometer (MODIS)

4 We retrieved MODIS reflectances, VIs and other products from the USGS repository covering the four  
5 eddy flux locations. Data were subject to quality assurance (QA) filtering, and pixels sampled during  
6 cloudy conditions and pixels adjacent to cloudy pixels were rejected (for a complete list of QA rules  
7 see Supplement Table 1). Other QA datasets and/or fields related to the above products that were not  
8 included on the original metadata were not examined as part of the quality filtering process.

9 At each site we extracted either a 1 km window (or a 1.25 km window depending on MODIS product  
10 resolution – see Table 2) centred on the location of the flux tower. The mean and standard deviation of  
11 all pixels were assumed to be representative of the ecosystem. The derivative data collection included  
12 the following MODIS data (also see Table 2):

13 MCD43A1: The 8-day 500m (Collection 5) Nadir Bidirectional Reflectance Distribution Function  
14 (BRDF) Adjusted Reflectance (NBAR) product was used to derive the enhanced vegetation index  
15 ( $EVI_{SZA30}$ ) and the normalized vegetation index ( $NDVI_{SZA30}$ ) at fixed solar zenith angle of 30° (available  
16 for 2003 to 2013):

$$17 \quad NDVI_{SZA30} = \frac{NIR_{SZA30} - R_{SZA30}}{NIR_{SZA30} + R_{SZA30}} \quad (10)$$

$$18 \quad EVI_{SZA30} = \frac{G \times (NIR_{SZA30} - R_{SZA30})}{NIR_{SZA30} + (C1 \times R_{SZA30}) - (C2 \times B_{SZA30}) + L} \quad (11)$$

1 where  $R_{SZA30}$ ,  $NIR_{SZA30}$  and  $B_{SZA30}$  are the red, near infrared, and blue band BRDF corrected reflectances,  
2 and coefficients  $G=2.5$ ,  $C1=6$ ,  $C2 = 7.5$ , and  $L=1$  (Huete et al., 1994). Both VIs are measures of  
3 greenness and have been designed to monitor vegetation, in particular photosynthetic potential and  
4 phenology (Huete et al., 1994; Running et al., 1994). However, the *EVI* has been optimized to  
5 minimize the effects of soil background, and to reduce the impact of residual atmospheric effects.

6 We labelled the NBAR VIs as  $EVI_{SZA30}$  and  $NDVI_{SZA30}$  to differentiate them from the MOD13 VI product  
7 (*EVI* and *NDVI*), and emphasize the values here presented include a BRDF correction that is aimed to  
8 remove the influence of sun-sensor geometry on the reflectance signal (Schaaf et al., 2002).

9 MOD15A2: The Leaf Area Index ( $LAI_{MOD}$ ), and Fraction of Photosynthetically Active Radiation  
10 ( $fPAR_{MOD}$ ) absorbed by vegetation from atmospherically corrected surface reflectance products  
11 (Knyazikhin et al., 1999). Data were filtered to remove outliers present in the  $fPAR_{MOD}$  and  $LAI_{MOD}$  time  
12 series using Eq. 3. A threshold value of 6 for the z coefficient was calibrated to remove 8-day  
13 variations of  $\pm 50\%$  on  $fPAR_{MOD}$ , and  $\pm 3-4$  units in  $LAI_{MOD}$ .

14 MOD17A2: The 8-day Gross Primary Production ( $GPP_{MOD}$ ) and Net Photosynthesis (*PsnNet*)  
15 (collection 5.1). The  $GPP_{MOD}$  is calculated using the formulation proposed by Running et al. (2000)  
16 and relies on satellite derived short-wave downward solar radiation ( $SW_{down}$ ),  $fPAR_{MOD}$ , maximum light-  
17 use-efficiency ( $\epsilon_{max}$ ) obtained from a biome-properties look-up table, and maximum daily *VPD*  
18 ( $VPD_{max}$ ) and minimum daily air temperature ( $T_{min}$ ) from forcing meteorology:

$$19 \quad GPP_{MOD} = \epsilon_{max} \times 0.45 \times SW_{down} \times fPAR_{MOD} \times f(VPD_{max}) \times f(T_{min}) \quad (12)$$

1 where only the highest quality data were selected for the analysis.

2 MOD11A2: Daytime Land Surface Temperature ( $LST_{day}$ ) 8-day time-series was included in the analysis  
3 in order to study the effect of  $T_{air}$ , another important ecosystem carbon flux driver. Thus, as  $LST$  or skin  
4 temperature (temperature at the interface between the surface and the atmosphere) has been proven to  
5 be highly correlated to  $T_{air}$  (Shen and Leptoukh, 2011).

### 6 **2.3.2. Satellite measures of precipitation (TRMM) and incoming solar radiation (CERES)**

7 This study incorporated monthly 0.25 degree resolution precipitation data (1998-2013) in units of mm  
8 month<sup>-1</sup> from the Tropical Rainfall Measuring Mission (TRMM) data product (3B43-v7) derived by  
9 combining TRMM satellite data, GOES-PI satellite data, and a global network of gauge data (Huffman  
10 et al., 2007). We used 1.0° resolution monthly surface shortwave flux down (all-sky) in  $W\ m^{-2}$  from the  
11 Clouds and the Earth's Radiant Energy System (CERES) experiment (Gesch et al., 1999). The CERES  
12 Energy Balanced And Filled top of the atmosphere (EBAF) Surface\_Ed2.8 product provided fluxes at  
13 surface, consistent with top of the atmosphere fluxes (CERES- EBAF TOA) (Kato et al., 2012). No  
14 quality control was performed on the rain ( $Precip_{TRMM}$ ) or short wave ( $SW_{CERES}$ ) satellite derived time  
15 series. We used satellite derived meteorological variables instead of in situ measurements as the  
16 independent variable in  $GEP$  models (see Section 2.5), thus, our findings (e.g. regressions) can be  
17 extrapolated to regional and continental scales.

### 18 **2.4. Mean values**

19 All analyses were done on 16-day data, therefore, 8-day MODIS products were resampled to the match  
20 the selected temporal resolution. We interpolated lower frequency satellite remote sensing time series  
21 (e.g. CERES and TRMM), using a linear regression from the original dataset to 16-days, where the  
22 original value corresponds to the centre of the month defined as day 15, and the newly interpolated



1 value will be representative of the middle of the 16-day period.

2 Mean fluxes and variables from the eddy covariance are reported on a 30-minutes or hourly basis.

3 Daily averages were calculated if at least 45 out of 48, or 21 out of 24 data points were available for the  
4 day. Bi-weekly values were calculated if at least 4 out of the 16 days were available. For analysis and  
5 presentation purposes, we averaged all existing 16-day values of EC and RS data to produce a single  
6 year, seasonal cycle. We understand measures of photosynthetic potential as to be dependent of the  
7 selection of aggregation period. However, the 16-day interval has been shown to be representative of  
8 important ecological processes, in particular, leaf appearance to full expansion (Jurik, 1986; Varone and  
9 Gratani, 2009), greenup of soil biological crusts in response to precipitation events (Cleverly et al.,  
10 2016a), and reported ecosystem-level changes in ecosystem water use efficiency (Shi et al., 2014).

## 11 **2.5. Evaluation of synchronicity between remote sensing and flux-tower data**

12 We fitted Type II (orthogonal) linear regressions that account for uncertainty in both variables (satellite  
13 and EC). We obtained an array of very simple models of productivity and photosynthetic potential.  
14 For example,  $GEP_{RS}$ , where  $GEP_{RS} = b_0 + b_1 \times RS$ ,  $b_0$  and  $b_1$  were site-specific coefficients, and RS are  
15 satellite derived products ( $EVI$ ,  $fPAR$ , etc.). We compared the different models to the observations  
16 ( $GEP$  versus  $GEP_{EVI}$ ,  $GEP$  versus  $GEP_{NDVI}$ , etc.) using Taylor single diagrams (Taylor, 2001), where the  
17 radial distances from the origin are the normalized standard deviation, and the azimuthal position is the  
18 correlation coefficient between the  $GEP_{RS}$  and  $GEP$  or any other measure of ecosystem photosynthetic  
19 potential (Supplement Fig. 2).

20 We determined at each site which combination of carbon flux and MODIS index showed good  
21 agreement based on statistical descriptors: coefficient of determination, p-value, root-mean-square-

1 error (RMSE), standard deviation (SD) of the observation and model, and the Akaike's Information  
2 Criterion (AIC). Thus, we analysed site-specific and cross-site multiple regression models to compare  
3 different biological (greenness) and environmental controls (precipitation, temperature, and radiation)  
4 on productivity. In each ecosystem, *GEP* was modelled as a linear regression using a single  
5 independent variable, two-variables, and bivariate models that included an interaction term. For  
6 example: (1)  $GEP = b_0 + b_1 \times EVI_{SZA30}$ , (2)  $GEP = b_0 + b_1 \times EVI_{SZA30} + b_2 \times SW_{CERES}$ , and (3)  $GEP = b_0 +$   
7  $b_1 \times EVI_{SZA30} + b_2 \times SW_{CERES} + b_3 \times EVI_{SZA30} \times SW_{CERES}$ , where  $b_0$ ,  $b_1$ ,  $b_2$ , and  $b_3$  were fitted coefficients by  
8 the non-linear mixed-effects estimation method. Additional models derived from the all-site  
9 regressions were compared to the site-specific results. We inferred ecosystem adaptation responses to  
10 climate (e.g. light harvest adaptation, water limitation, among other phenological responses) from the  
11 bivariate models. This analysis is useful for the interpretation of satellite derived phenology metrics  
12 and understanding the biophysical significance of different measures of greenness when incorporated  
13 into land surface models as representative of vegetation status (Case et al., 2014).

### 14 **3. Results**

#### 15 **3.1. Seasonality of in situ measurements**

16 In this section we describe the seasonality of in situ meteorological measurements to better understand  
17 ecosystem carbon fluxes, and to contextualize the differences in vegetation responses to climate. In  
18 particular, we contrast seasonal patterns of air temperature ( $T_{air}$ ), precipitation, and *VPD* across sites,  
19 and compare observations of the annual cycle of photosynthetic activity (productivity) and potential  
20 (biophysical drivers of productivity) for each ecosystem.

21 With the exception of AU-How, all sites showed strong seasonality in  $T_{air}$  (Fig. 3). However, the timing  
22 of mean daily  $T_{air}$  minimum and maximum, and the amplitude of the annual values, varied according to  
23 site. The smallest range in  $T_{air}$  (5°C) occurred at the northern tropical savanna (AU-How), and the

1 largest amplitude ( $15^{\circ}\text{C}$ ) occurred at the southern temperate locations (AU-Cpr and AU-Tum). The  
2 annual cycle of  $VPD$  followed  $T_{air}$  at all locations except AU-How where summer and autumn rains  
3 (February-March) lead to a increase in atmospheric water content (Figure 3). Precipitation at AU-How  
4 was higher and more seasonal than at any other site with a mean monthly rainfall of 152 mm (1824 mm  
5 year<sup>-1</sup>) and ranging from 1 to 396 mm month<sup>-1</sup>. Incoming radiation at the tropical savanna site (AU-  
6 How) did not show clear seasonality (Figure 3). In this tropical savanna (latitude  $12.49^{\circ}\text{S}$ ) the summer  
7 solstice, where top of the atmosphere (TOA) radiation is highest, coincides with monsoonal cloudiness  
8 resulting in reduced surface radiation. By contrast, at temperate sites like AU-Cpr and AU-Tum, the  
9 difference in mean daily  $PAR$  between summer and winter was  $\sim 460 \mu\text{mol m}^{-2} \text{s}^{-1}$ . Rainfall was  
10 aseasonal at AU-Tum ( $\sim 78 \text{ mm month}^{-1}$ ) and was very low at the semi-arid sites of AU-Cpr and AU-  
11 ASM with mean precipitation values of 34 and 37 mm month<sup>-1</sup> respectively.

12 Productivity in the four ecosystems ranged from a high at AU-How and AU-Tum (Figure 4) (peak 16-  
13 day multi-year average  $GEP$  of 8.4 and 7.7  $\text{gC m}^{-2} \text{d}^{-1}$  respectively) to a low at AU-Cpr and AU-ASM  
14 (peak 16-day annual average  $GEP$  average of 2.4 and 3.4  $\text{gC m}^{-2} \text{d}^{-1}$  respectively) (Figure 4). There  
15 was a clear seasonal cycle in photosynthetic activity with maxima in the summer at AU-How and AU-  
16 Tum (November-March) and in the autumn (March-April) at AU-ASM and AU-Cpr. The peaks were  
17 broader at AU-Tum than at AU-How and at AU-ASM (Figure 4). An additional short-lived increase in  
18  $GEP$  was apparent at AU-ASM in the spring (October) before the summer wet period (Figure 4a).  
19 Supplement Figures 3 and 4 show the diel cycles of  $VPD$ ,  $GEP$  and other meteorological and flux  
20 variables in example summer (January) and winter months (July).

21 Vegetation phenology, as indicated by the seasonal cycle of photosynthetic potential ( $P_c$ ,  $LUE$ ,  $\alpha$ , and  
22  $GEP_{sat}$ ), diverged from photosynthetic activity ( $GEP$ ) at the southern locations of AU-Tum and AU-Cpr  
23 as shown by the differences in the timing of maximum and minimum  $GEP$  compared to vegetation

1 phenology (Figure 4 and Supplement Fig. 5). At the tropical savanna site (AU-How), ecosystem  
2 quantum yield ( $\alpha$ ) increased gradually in the spring (September), reaching a maximum during the  
3 summer month of January in synchrony with  $GEP$ . In the sclerophyll forest (AU-Tum),  $\alpha$  remained at  
4 a constant value of  $\sim 1.4 \text{ gC MJ}^{-1}$  until the middle of the autumn (April-May) when it reached a value of  
5  $1.76 \text{ gC MJ}^{-1}$ . Maximum  $GEP_{sat}$  occurred during the summer at this site ( $\sim 36 \text{ gC m}^{-2} \text{ d}^{-1}$ ) and gradually  
6 decreased by the start of the autumn with a winter minimum ( $20 \text{ gC m}^{-2} \text{ d}^{-1}$ ). At AU-Tum, the  $GEP_{sat}$   
7 and  $\alpha$  were out-of-phase (Figure 4) and although seasonality was limited in  $GEP_{sat}$  and  $\alpha$ , neither of  
8 them matched seasonal fluctuations in  $VPD$  (cf. Figures 3 and 4). Similar to  $GEP_{sat}$ ,  $LUE$  decreased  
9 during the summer months and experiences a winter maximum opposite to the annual cycle of  $GEP$ .  
10 Given the high degree of seasonality of  $GEP$  at AU-Tum, it is interesting that the photosynthetic  
11 potential was comparatively less seasonal and asynchronous to productivity. Supplement Fig. 5 shows  
12 the relationships between the different measures of ecosystem performance indicating that they are not  
13 always linear.

### 14 **3.2. Seasonality of satellite products**

15 In the tropical savanna (AU-How) the annual cycles of RS products synchronously reached an early  
16 summer maximum in January, and high values extended throughout the autumn (Figure 4d and e). By  
17 contrast at AU-Cpr, both  $NDVI_{SZA30}$  and  $EVI_{SZA30}$  peaked in autumn-winter, coinciding with the lowest  
18  $GEP$  values (Figure 4p and s).  $EVI_{SZA30}$  and  $NDVI_{SZA30}$  at AU-ASM captured the autumn peak in  $GEP$   
19 with a maximum in March, however, a spring VI minimum (November) was not observable in  $GEP$ .  
20 At the two semi-arid sites (AU-ASM and AU-Cpr),  $fPAR_{MOD}$  was relatively aseasonal, and the  
21 amplitude of the annual cycle was  $\sim 0.09$ , with a 0.25-0.34 range at AU-Cpr and lower values between  
22 0.17-0.26 at AU-ASM (Figure 4o).  $LAI_{MOD}$  at AU-Cpr reached a maximum of 0.50 during the autumn  
23 (March) and a spring minimum (September) of 0.39. At AU-ASM, the  $LAI_{MOD}$  product ranged from  
24 0.17 (December) to 0.27 (April) (Figure 4t). Most RS products (e.g.  $EVI_{SZA30}$  and  $LAI_{MOD}$ ) showed no

1 clear seasonality at AU-Tum (Figure 5i and j).

2  $fPAR_{MOD}$  versus  $NDVI_{SZA30}$  were highly correlated at all sites ( $R^2 > 0.7$ ,  $p < 0.01$ ) with the exception of the  
3 sclerophyll forest (AU-Tum) where  $NDVI_{SZA30}$  remained constant in the 0.68 - 0.83 range ( $R^2 = 0.01$ )  
4 (Supplement Fig. 6). At the sclerophyll forest site (AU-Tum), the  $NDVI_{SZA30}$  reached values close to  
5 saturation. Similar to  $fPAR_{MOD}$  versus  $NDVI_{SZA30}$ ,  $EVI_{SZA30}$  versus  $NDVI_{SZA30}$  was highly correlated  
6 ( $R^2 = 0.96$ , all-site regression). However, the timing of minimum and maximum between  $NDVI_{SZA30}$  and  
7  $EVI_{SZA30}$  differed at AU-Cpr and AU-How (Figure 4 and Figure 5d and s).

### 8 **3.3. Relationship between MODIS *EVI* and *GPP* and in situ measures of ecosystem** 9 **photosynthetic activity (*GEP*)**

10 In this study we used a simple linear model to predict  $GEP$  from  $EVI_{SZA30}$  and  $GPP_{MOD}$ . We observed  
11 three patterns. First, in the tropical savanna site (AU-How) there was a highly significant correlation  
12 between photosynthetic activity and  $EVI_{SZA30}$ , where  $EVI_{SZA30}$  explained 82% of  $GEP$  (Figure 5a).  
13 Similarly at AU-ASM, productivity was statistically related to  $EVI_{SZA30}$  ( $R^2 = 0.86$ ,  $p < 0.01$ ). However,  
14  $GPP_{MOD}$  only explained 49% of  $GEP$  at AU-How and 48% at AU-ASM (Figure 5e and g).

15 A second pattern was observed in the sclerophyll forest site (AU-Tum), where the relationship between  
16  $GEP$  and  $EVI_{SZA30}$  was not statistically significant ( $R^2 < 0.01$  and  $p = 0.93$ , Figure 5b). At AU-Tum there  
17 was a clear seasonal cycle in  $GEP$  (low in winter and high during the summer) that was not captured by  
18 the small amplitude of the satellite derived data (Figure 3). Of the four ecosystems examined, AU-Tum  
19 was the only site where  $GPP_{MOD}$  showed an improvement (higher predictive value of  $GEP$ ) compared  
20 to  $EVI_{SZA30}$ . However, as reported in previous works (Leuning et al., 2005), the  $GPP_{MOD}$  product was  
21 unable to capture the seasonality of the sclerophyll forest as it underestimated the observed summer  
22 peak in  $GEP$  which corresponded to a second minimum in  $GPP_{MOD}$ .

1 Finally, at the semi-arid site (AU-Cpr), we observed  $R^2$  values significantly different from 0 but small  
2  $R^2$  0.34 and 0.24 ( $p < 0.01$ ) for *GEP* versus  $EVI_{SZA30}$  and *GEP* versus  $GPP_{MOD}$ , respectively. This,  
3 demonstrated the low predictive power of both satellite products to determine seasonal *GEP* values at  
4 this particular Mediterranean ecosystem. In particular the  $GEP_{EVI}$  and  $GPP_{MOD}$  models tended to  
5 underestimate productivity at low levels (Figure 5d and h).

6 The relationship between productivity and  $EVI_{SZA30}$  was complex across the different Australian  
7 ecosystems (Figure 5). The semi-arid site of AU-Cpr and the sclerophyll forest of AU-Tum are  
8 particularly interesting because of the inability of  $EVI_{SZA30}$  to seasonally replicate *GEP* (Figure 5). An  
9 additional analysis that considers the amplitude and phase of the annual cycle (based on all available  
10 16-day observations) was conducted using Taylor plots (Supplement Fig. 7). This analysis showed that  
11  $EVI_{SZA30}$  was in-phase and able to predict the range of productivity values at AU-How and AU-ASM,  
12 while at the AU-Cpr site the  $EVI_{SZA30}$  captured the amplitude of seasonal *GEP*, however, the linear  
13 model was out-of-phase. At AU-Tum, the  $EVI_{SZA30}$ -based model consistently preceded in situ  
14 observations (asynchronous) and exaggerated *GEP* seasonality (ratio between the standard deviation of  
15 the model and observations was 4.98).

### 16 **3.4. Relationship between $EVI_{SZA30}$ and measures of photosynthetic potential ( $\alpha$ , $LUE$ , $GEP_{sat}$ , 17 and $Pc$ )**

18 In this section we reconsider our understanding of  $EVI_{SZA30}$  by relating it to different measures of  
19 photosynthetic potential ( $\alpha$ ,  $LUE$ ,  $GEP_{sat}$ , and  $Pc$ ) across the four sites (Figure 6). Similar to section  
20 3.3, we used a very simple linear model in which  $EVI_{SZA30}$  was expected to predict  $\alpha$ ,  $LUE$ ,  $GEP_{sat}$ , and  
21  $Pc$ . In the regression models for photosynthetic potential the  $R^2$  values were similar to the *GEP* models  
22 for AU-How and AU-ASM (cf. Figure 6c and g). However,  $EVI_{SZA30}$  versus  $\alpha$  at AU-How  $R^2$  was

1 relatively low ( $R^2 < 0.4$ ,  $p < 0.01$ ). At the AU-Cpr site, the  $EVI_{SZA30}$ -based model was able to improve the  
2 timing and amplitude of the annual cycle when used to calculate  $LUE$ ,  $Pc$  and  $GEP_{sat}$  instead of  $GEP$   
3 (Figure 6 and Supplement Fig. 7).

4 At the sclerophyll forest site (AU-Tum) the  $EVI_{SZA30}$  was able to predict vegetation phenology rather  
5 than productivity. For example we observed that  $Pc$  (but not  $\alpha$ ) was significantly related to  $EVI_{SZA30}$   
6 ( $R^2 = 0.16$ ,  $p < 0.01$ ; Figure 6 and Supplement Table 4). Even though, the regressions between  $LUE$ ,  
7  $GEP_{sat}$ , and  $Pc$  against  $EVI_{SZA30}$  showed higher correlation ( $R^2 \sim 0.13$ ,  $p < 0.01$ ) than the  $GEP$  versus  
8  $EVI_{SZA30}$  relationship ( $R^2 = 0.04$ ,  $p = 0.25$ ) at AU-Tum,  $R^2$  values were still low. The low  $R^2$  can be  
9 explained by the small dynamic range of both seasonal measures of photosynthetic potential and  
10  $EVI_{SZA30}$  (cf. Figures 4 and 6).

### 11 **3.5. Satellite products compared to flux tower based measures of ecosystem potential**

12 In this section we explore other MODIS products ( $LAI_{MOD}$ ,  $fPAR_{MOD}$ , and  $NDVI_{SZA30}$ ) to determine if the  
13 predictive power of  $EVI_{SZA30}$  as a measure of photosynthetic potential (e.g.  $Pc$ ) can be generalised  
14 across other satellite-derived biophysical parameters. We aimed to determine for each location, which  
15 of the MODIS products capture the seasonality and phenology of vegetation, thereby gaining some  
16 insight into the significance of the different VIs and other satellite derived ecosystem drivers. At AU-  
17 How and AU-ASM the MODIS  $LAI_{MOD}$ ,  $fPAR_{MOD}$ , and VIs showed a larger or similar correlations to  
18  $LUE$  and  $Pc$  in comparison to  $GEP$  (Supplement Table 4, Figure 7a and b and Figure 7i and j,  
19 respectively). At AU-How, AU-ASM, and AU-Cpr, based on our analysis using Taylor plots, most RS  
20 products were in-phase with the various measures phenology ( $R^2 > 0.8$  and low RMSE) (Figure 7 and  
21 Supplement Figure 2 and Table 4). However, there was a tendency for most RS indices to  
22 underestimate the seasonality of the  $LUE$  annual cycle at all sites (i.e., standard deviation was smaller  
23 for  $LUE_{RS}$  than the observed, Figure 7). With exception to AU-Tum, all products were able to capture

1 seasonal changes in  $P_c$  (Figures 6 and 7).

2 Similar to  $EVI_{SZA30}$ , most of the MODIS indices, and in particular  $fPAR_{MOD}$  and  $LAI_{MOD}$ , showed strong  
3 linear relationships with  $LUE$  and  $P_c$  at the Mediterranean ecosystem AU-Cpr, where the introduction  
4 of phenology represented an important improvement over the RS-derived models (Figures 6 and 7).  
5 Similarly, comparable to  $EVI_{SZA30}$ , other MODIS products were unable to replicate  $GEP$  at AU-Tum  
6 (Figure 7). However, the small amplitude of seasonality in  $LUE$  and  $P_c$  were well characterized by  
7  $LUE_{RS}$  and  $P_{CRS}$ , including a winter maximum similar to that in  $LUE$  (Figure 4), despite underestimating  
8 the annual seasonal cycle in the sclerophyll forest (Figures 4 and 7e-h).

### 9 **3.6. Multi-biome derived linear relationships between VIs and photosynthetic potential** 10 **(phenology) and activity (productivity)**

11 Our objective was to investigate if one relation fits all flux sites, and which RS products and equations  
12 would enable us to extend our analysis from these four key Australian ecosystems to a continental  
13 scale. The all-site relationship for MODIS  $EVI_{SZA30}$ ,  $NDVI_{SZA30}$ ,  $LAI_{MOD}$ , and  $fPAR_{MOD}$  products (in that  
14 order) show the best agreement (phase and amplitude) to seasonality of  $LUE$  and  $P_c$  (Figure 7).  
15 Correlations increased for relationships built using data for all the ecosystems instead of the site-  
16 specific equations with the exception of the AU-ASM site (Table 3 and Figures 7 and 8).

17 Improvements in how satellite products can model biological drivers (photosynthetic potential) instead  
18 of productivity *per se*, are clearly seen at the evergreen temperate forest of AU-Tum. At AU-Tum the  
19 relationship between  $GEP$  and any of the satellite products was not statistically significant ( $R^2 < 0.1$ )  
20 with the exception of  $LST_{day}$  (Figures 5 and 7). However, skin temperature ( $LST_{day}$ ) is a meteorological  
21 driver rather than a direct measure of productivity, and the low all-site  $LST_{day}$  versus  $GEP$  correlation  
22 was an indication of this ( $R^2=0.66$ ,  $p=0.03$ ; Figure 8).



1 The wet sclerophyll forest introduced the greatest uncertainties to the linear models across all sites  
2 (Figure 8). For example, regressions involving  $EVI_{SZA30}$  were exponential, therefore, significantly  
3 increasing  $GEP$  and  $LUE$  translated into slightly higher  $EVI_{SZA30}$  values, a behaviour mostly driven by  
4 the observations at AU-Tum. In particular, the relationship between  $LUE$  versus  $fPAR_{MOD}$  and  $LUE$   
5 versus  $NDVI_{SZA30}$  at AU-Tum were problematic as  $fPAR_{MOD}$  and  $NDVI_{SZA30}$ , appeared to “saturate” at 0.9  
6 and 0.8, respectively (Figure 8).

7  $EVI_{SZA30}$  explained 81% of  $Pc$  seasonality based on an all-site regression (Supplement Table 4).  
8 Similarly,  $NDVI_{SZA30}$  showed a high coefficient of determination (0.70 for  $GEP_{NDVI}$ , 0.75 for  $LUE_{NDVI}$ ,  
9 and 0.79 for  $Pc_{NDVI}$ ) (Supplement Table 4). The null hypothesis of no correlation was rejected ( $p < 0.01$ )  
10 for all regressions between MODIS VIs,  $LAI_{MOD}$  and  $fPAR_{MOD}$  versus photosynthetic potential  
11 (phenology) and activity (productivity) (Supplement Table 4). However, statistical significance of  
12  $GEP$  versus  $GEP_{RS}$ , was driven by the AU-ASM and AU-How ecosystems.

13 Multiple linear regression models used to predict  $GEP$  by combining satellite derived meteorology and  
14 biologic parameters (Table 3) showed large correlations when both drivers were introduced (weather  
15 and vegetation phenology), with the exception of the AU-Tum site where  $SW_{CERES}$  and  $LST_{day}$  explained  
16 60% and 58% of  $GEP$ , respectively, and the AU-ASM and AU-How sites where  $EVI_{SZA30}$  and  $NDVI_{SZA30}$   
17 explained ~84% and ~80% of the variations in  $GEP$ , respectively. In particular, at the AU-How site, no  
18 significant improvement to the  $GEP$  model was obtained when combining MODIS VIs with any  
19 meteorological variable ( $R^2$  remain similarly high  $R^2 \sim 0.82$ ). By contrast, at the AU-ASM site,  $EVI_{SZA30}$ ,  
20 satellite derived incoming short wave ( $SW_{CERES}$ ), and the interaction of both significantly increased  
21 model correlation with an  $R^2$  of 0.88 and a lower AIC (Akaike’s Information Criterion as a measure of  
22 model quality) when compared to models relying only on  $EVI_{SZA30}$  ( $R^2 = 0.85$ ,  $AIC = 64$ ) or  $SW_{CERES}$

1 ( $R^2=0.02$ , AIC =209) (Table 3). Similar results were obtained for those regressions driven by  $EVI_{SZA30}$   
2 and precipitation at this rainfall pulse driven site ( $R^2=0.88$ , AIC=42). At the AU-Cpr site, temperature-  
3 greenness models were highly correlated to  $GEP$  ( $R^2>0.64$ ), however, the best results (higher  $R^2$  and  
4 lower AIC) were obtained for radiation-greenness models, explaining 71% ( $EVI_{SZA30} - SW_{CERES}$  and  
5  $NDVI_{SZA30} - SW_{CERES}$ ) of  $GEP$ . For a complete version of Table 3 that includes all available variable  
6 combinations, see Supplement Table 3.

## 7 **4. Discussion**

### 8 **4.1. Derivation of measures of photosynthetic potential at tropical savannas, sclerophyll forests** 9 **and semi-arid ecosystems**

10 In this study we were able to separate the biological (vegetation phenological signal) from the climatic  
11 drivers of productivity using eddy-covariance carbon exchange data. Using the parameterization of the  
12 light response curve we derived different measures of vegetation photosynthetic potential ( $\alpha$ ,  $LUE$ ,  
13  $GEP_{sat}$  and  $Pc$ ) (Balzarolo et al., 2015; Wohlfahrt et al., 2010). At seasonal time scales (e.g. 16-days,  
14 monthly), our analysis looks at the biotic drivers of productivity; whereas at shorter time scales (e.g.  
15 hourly, daily) photosynthetic potential can be limited or enhanced by meteorological controls, thus as  
16 linked to resource scarcity (i.e. high  $VPD$  or water constraints), or availability (e.g. increase radiation or  
17 access to soil water), and correspondent ecosystem responses (e.g. stomatal closure,  $CO_2$  fertilization)  
18 will determine  $GEP$  (Ainsworth and Long, 2005; Doughty et al., 2014; Fatichi et al., 2014). The  
19 variables  $\alpha$ ,  $LUE$ ,  $GEP_{sat}$ , and  $Pc$  have different biophysical meanings; therefore, we were able to  
20 establish physiological explanations for describing why and which RS products and environmental  
21 variables relate to them at each ecosystem. For example,  $GEP_{sat}$  measured at high levels of  $PAR$  is  
22 prone to be influenced by various environmental factors ( $VPD$ ,  $T_{air}$  and soil water availability) and  
23 therefore may be a good indicator of canopy stress.

1 As observed at AU-How,  $GEP_{sat}$  was highly and negatively correlated to periods of low precipitation  
2 and negatively correlated with VPD (Supplement Table 4). Seasonal values of  $GEP_{sat}$  at the semi-arid  
3 sites (AU-Cpr and AU-ASM) did not show a direct relationship with VPD or precipitation. This does  
4 not mean that there is no effect of atmospheric demand or soil moisture content on carbon fluxes at  
5 shorter time scales (hourly or daily) (Cleverly et al., 2016b; Eamus et al., 2013). Compared to  $GEP_{sat}$ ,  
6 we expected  $\alpha$  to be less dependent of VPD and better reflect vegetation phenology, as  $\alpha$  represents the  
7 canopy photosynthetic response at low levels of PAR characteristic of cloud cover (diffuse light) during  
8 early morning or late afternoon periods (Kanniah et al., 2012, 2013). However, among all measures of  
9 phenology,  $\alpha$  showed one of the lowest site-specific correlations when compared to any of the RS  
10 products presented on this study. Our results show that  $LUE$  and  $Pc$  showed the best correlations to  
11 VIs. Confirmation that this research deals less with the instantaneous responses ( $GEP_{sat}$  and  $\alpha$ ) and  
12 rather focuses on the mid-term, 16-day seasonal descriptors of vegetation phenology ( $Pc$  and  $LUE$ ).

13 The influence of other environmental factors apart from PAR and VPD, such as soil water content and  
14  $T_{air}$ , is difficult to isolate from the derivation of vegetation descriptors as there may be a high degree of  
15 cross-correlation between the different variables (e.g. VPD versus  $T_{air}$ ). Moreover, to what degree it is  
16 feasible to untangle the relations between climate and vegetation is complex and not well understood,  
17 as the feedback processes are essential in ecosystem function (leaf flush, wood allocation, among other  
18 vegetation strategies respond to available resources), species competition, and herbivory cycles  
19 (Delpierre et al., 2015). Our results show that VIs were highly related to  $Pc$ , which is interpreted as a  
20 phenology descriptor that does not consider the day-to-day changes in available light or photoperiod or  
21 the vegetation response to high and low VPD and PAR values. By contrast, implicit in the derivation of  
22  $LUE$  were the day length and anomalous climatic conditions. This finding has important implications  
23 when using EC data for the validation of satellite derived phenology (Restrepo Coupe et al., 2015).

1 **4.2. Seasonality and comparisons between satellite products and flux tower based measurements**  
2 **of carbon flux: photosynthetic activity (productivity) and potential (phenology)**

3 Previous satellite derived models of productivity usually apply to locations where the seasonality of  
4 *GEP* is synchronous with climatic and vegetation phenology drivers (Mahadevan et al., 2008; Sims et  
5 al., 2008; Wu et al., 2010; Xiao et al., 2004), such as in temperate deciduous forests, where temperature  
6 and incoming radiation coincide with changes in ecosystem structure and function (e.g. autumn sub-  
7 zero temperatures may initiate leaf abscission (Vitasse et al., 2014)). In our analysis, productivity was  
8 synchronous with all measures of photosynthetic potential only at the savanna site (AU-How), where  
9 clouds and heavy rainfall in the summer wet season resulted in low *VPD*, reduced *TOA* (aseasonal  
10 *PAR*), and minimal fluctuations in  $T_{air}$ . At AU-How, we observed a consistently large correlation  
11 between MODIS VIs and productivity and no improvement in *GEP* when accounting for meteorology.  
12 Moreover, the highly significant *EVI*<sub>SZA30</sub> versus *GEP* relationship at AU-How could be generalised to  
13 other satellite derived biophysical products.

14 Arid and semi-arid vegetation dominate ~75% of the Australian continent, and at these ecosystems a  
15 characteristic mix of grasses (understory) and woody plants (overstory) contribute to total annual *GEP*  
16 at different times of the year. More importantly, the phenology of grasses and trees are driven by, or  
17 respond differently to, various climatic drivers (e.g. trees greening up after spring rainfalls while  
18 grasses remain dormant (Cleverly et al., 2016a; Ma et al., 2013; Shi et al., 2014). The changing  
19 seasonal contributions to the reflectance signal and to *GEP* are generally related to soil water content  
20 thresholds. Our study presents two semi-arid *Acacia* and *Eucalyptus* woodlands where we found that  
21 models relating VIs with photosynthetic potential (phenology), rather than activity (productivity),  
22 improved the predictive power of RS greenness indices (AU-Cpr) or showed similar statistical  
23 descriptors (AU-ASM). At the woodland *Acacia* site,  $LAI_{MOD}$  and  $fPAR_{MOD}$  overestimated the periods of  
24 low capacity (associated with browndown phases) (Ma et al., 2013). This can be better understood if

1 we account for small but non-negligible photosynthetic activity in *Acacia* after the summer rains have  
2 ended (Cleverly et al., 2013; Eamus et al., 2013). At this particular site (AU-ASM), the high  $LAI_{MOD}$   
3 and VIs observed during dormancy may not be interpreted as high photosynthetic potential. Satellite  
4 data, and even some ground-based measurements of  $LAI_{MOD}$ , cannot differentiate between the different  
5 fractional components: photosynthetic active vegetation ( $fPAV$ ), and non-photosynthetic vegetation  
6 ( $fNPV$ ). Future work requires phenocams or biomass studies in which  $fPV$  and  $fNPV$  may be spectrally  
7 or mechanically separated.

8 In low productivity ecosystems (AU-ASM and AU-Cpr), satellite and EC data/noise ratio may have a  
9 considerable effect on the site-specific regressions (e.g. sun geometry influence on VIs seasonal values,  
10 and EC uncertainties). However, differences between AU-ASM and AU-Cpr regressions (e.g.  $EVI_{SZA30}$   
11 was highly correlated to  $GEP$  only at AU-ASM) and the fact that the VI product has been corrected for  
12 BRDF effects, increases our confidence on the analysis presented here. Moreover, the lower VIs  
13 versus  $GEP$  correlation values obtained at AU-Cpr compared to AU-ASM could be attributed to Mallee  
14 site productivity being more dependent on meteorological drivers than photosynthetic potential, or  
15  $GEP$  being driven by climate (e.g. autumn precipitation –when  $Pc$  remains constant) or by vegetation  
16 phenology (e.g. summer  $LAI$  and canopy chlorophyll content, among others) at different times of the  
17 year.

18 Similar to Mediterranean ecosystems (AU-Cpr), in wet sclerophyll forests (AU-Tum) without signs of  
19 water limitation, the VIs were unable to replicate seasonality in  $GEP$ . In particular, the dominant  
20 species of sclerophyll forests, *Eucalyptus*, *Acacias* and *Banksias*, show very little seasonal variation in  
21 canopy structure as seen in aseasonal  $LAI$  observations (Zolfaghar, 2013), and leaf longevity (Eamus et  
22 al., 2006). Leaf quantity (e.g.  $LAI$ ) and quality (e.g. leaf level photosynthetic assimilation capacity) are  
23 two key parameters in driving photosynthetic potential; when these are aseasonal, asynchronous or

1 lagged, they may confound the interpretation of seasonal measures of greening. Thus, the observed  
2 increasing predictive power of VIs as a measure of photosynthetic potential (e.g.  $EVI_{SZA30}$  versus  $Pc$ ,  
3  $R^2=0.16$  at AU-Tum) may not be comparable to similar relationships at sites where vegetation  
4 phenology showed a larger dynamic range (e.g.  $EVI_{SZA30}$  versus  $Pc$ ,  $R^2=0.79$  at AU-How).

#### 5 **4.3. Considerations for the selection of RS data to be used on GEP models and phenology** 6 **validation studies**

7 This study reports high correlations for  $Pc$  versus  $EVI_{SZA30}$  ( $R^2=0.81$ ) and  $Pc$  versus  $NDVI_{SZA30}$   
8 ( $R^2=0.80$ ). The fact that a brighter soil background results in lower  $NDVI$  values than with a dark soil  
9 background for the same quantity of partial vegetation cover (Huete, 1988; Huete and Tucker, 1991)  
10 may have a positive effect in the all-site  $Pc$  versus  $NDVI_{SZA30}$  regressions (increase  $R^2$ ). However,  
11 darkened soils following precipitation also raise  $NDVI$  values for incomplete canopies (Gao et al.,  
12 2000) and may similarly suggest higher vegetation or soil biological crust activity. On the other hand,  
13 soil brightness and moisture may have a negative effect on the confidence interval of the x-intercept for  
14 the proposed relationships (e.g.  $Pc$  versus  $NDVI_{SZA30}$ , for  $NDVI_{SZA30} \sim 0$ ). Moreover, at certain times the  
15 AU-ASM and AU-Cpr sites were at the low end of the vegetation activity range, and the observed RS  
16 signal may have been dominated by soil water content rather than by photosynthetic potential.  
17 However, caution is needed when using  $fPAR_{MOD}$  and other products as we observed a threshold value  
18 above which in situ changes were undetectable (e.g. MODIS  $fPAR > 0.9$ ,  $NDVI_{SZA30} > 0.8$ ). This might  
19 have been due to the  $NDVI$  saturating at high biomass (Huete et al., 2002; Santin-Janin et al., 2009).

20 Temperature-greenness models of  $GEP$  (Sims et al., 2008; Xiao et al., 2004) take into account the  
21 meteorological and biophysical drivers that determine productivity. Nevertheless, correlations between  
22 photosynthetic characteristics and  $LST_{day}$  were weaker than for VIs. Moreover, if the seasonality of  
23  $GEP$  is driven by local climatology, as in the case of AU-Tum where  $GEP$  was statistically correlated

1 to  $LST_{day}$ , our intent is to understand the relation between vegetation characteristics and RS products  
2 rather than indiscriminately use any satellite-derived index to describe phenology or photosynthetic  
3 potential. Our study demonstrates that multiple linear regression models that combine satellite derived  
4 meteorology and biological parameters to describe  $GEP$  fit better when both drivers are introduced  
5 rather than when only one factor drives the relation (a single meteorology or greenness variable).  
6 However, two exceptions to this rule were observed: (1) at AU-Tum where  $SW_{CERES}$  was able to explain  
7 60% of  $GEP$ , and (2) in the tropical savanna at AU-How where  $EVI_{SZA30}$  was able to explain ~82% of  
8 the variation in  $GEP$ , and where we did not obtain any significant improvement to the  $GEP$  model  
9 when combining MODIS VIs and any meteorological variable ( $R^2$  remain similarly high  $R^2 > 0.82$ ). In  
10 summary, at evergreen sclerophyll forests, even when  $GEP$  is highly seasonal,  $GEP$  is driven by  
11 meteorology as seen by the fact that most of the measures of photosynthetic potential showed small  
12 seasonal changes, similar to different MODIS products. By contrast, sites where most of the  $GEP$   
13 seasonality was driven by vegetation status ( $Pc$  as a proxy) rather than the meteorological inputs ( $PAR$ ,  
14 air temperature and precipitation), or where meteorology and phenology were synchronous, VIs were  
15 strongly correlated to both  $GEP$  and  $Pc$  (e.g. tropical savanna). This was in agreement with the  
16 expectation that RS products constitute a measurement of ecosystem photosynthetic potential rather  
17 than productivity *per se*.

18 Our analysis shows how MODIS greenness indices were able to estimate different measures of  
19 ecosystem photosynthetic potential across biomes. At only one site (AU-Tum) was there very little  
20 seasonal variation in  $EVI_{SZA30}$ , compared to other evergreen ecosystems. Both, the strong correlations  
21 among VIs and  $Pc$  from in situ EC carbon flux measurements at the remaining sites (AU-How, AU-  
22 ASM, and AU-Cpr), and the positioning of each ecosystem along a continuum of MODIS-derived  
23 variables representing vegetation phenology confirms the usefulness of satellite products as  
24 representative of vegetation structure and function. This research confirms the viability of remote

1 sensing-derived phenology to be validated and more importantly, understood, using eddy-flux  
2 measurements of  $P_c$ . However, an increase in effort in determining seasonal patterns of carbon  
3 allocation (partition between leaves and wood), understory and overstory responses, and leaf carbon  
4 assimilation and chlorophyll content over time, may be required to obtain a more meaningful  
5 understanding of RS indices and their biophysical significance. Moreover, the reader should be aware  
6 that rapid changes in vegetation phenology (e.g.  $\alpha$  and  $GEP_{sat}$ ) caused by short-term environmental  
7 stresses (e.g.  $T_{air}$ , humidity, soil water deficit, or waterlogging) may not be accurately estimated by RS  
8 products and require the employment of in situ high frequency optical measurements (e.g. phenocams),  
9 or land surface vegetation models, or direct EC measurements.

10 For this study we included all available 16-day data corresponding individually to more than 10 years  
11 at AU-How and AU-Tum, and two to three years at AU-Cpr and AU-ASM. The long-term sampling  
12 implies that we were likely to be capturing a large range in mean ecosystem behaviour. RS products  
13 may over- or under-represent the canopy response to periods of extreme temperature and precipitation,  
14 although the time series in this study included warmer than normal years and heat waves, e.g. 2012-  
15 2013 (BOM, 2012, 2013; van Gorsel et al., 2016) and wetter than normal years, e.g. 2011 (Fasullo et  
16 al., 2013; Poulter et al., 2014) that lead to larger than normal  $GEP$  at AU-ASM and AU-Cpr (Cleverly  
17 et al., 2013; Eamus et al., 2013; Koerber et al., 2016). It is beyond the scope of this work to evaluate  
18 the inter-annual variability of the vegetation responses to disturbance (e.g. insect infestation or fire) or  
19 extreme climatic events (e.g. flooding or long term drought). Improvements to satellite derived  
20 phenology can be related to an increasing number of EC sites and samples thereby emphasizing the  
21 importance of long-term time measurements and sampling of diverse ecosystems.

## 22 **5. Conclusions**

23 Satellite vegetation products have been widely used to scale carbon fluxes from eddy covariance (EC)



1 towers to regions and continents. However, at some key Australian ecosystems MODIS gross primary  
2 productivity ( $GPP$ ) product and vegetation indices (VIs) do not track seasonality of gross ecosystem  
3 productivity ( $GEP$ ). In particular, we found  $EVI_{SZA30}$  was unable to represent  $GEP$  at the temperate  
4 evergreen sclerophyll forest of Tumbarumba (AU-Tum) and at the Mediterranean ecosystem (Mallee)  
5 of Calperum-Chowilla (AU-Cpr). This result extends across satellite products overall: MODIS  
6  $GPP_{MOD}$ ,  $LAI_{MOD}$ ,  $fPAR_{MOD}$ , and other VIs.

7 We aimed for a greater understanding of the mechanistic controls on seasonal  $GEP$  and proposed the  
8 parameterization of the light response curve from EC fluxes, as a novel tool to obtain ground-based  
9 seasonal estimates of ecosystem photosynthetic potential (light use efficiency ( $LUE$ ), photosynthetic  
10 capacity ( $Pc$ ),  $GEP$  at saturation ( $GEP_{sat}$ ), and quantum yield ( $\alpha$ )). Photosynthetic potential refers to  
11 the presence of photosynthetic infrastructure in the form of ecosystem structure (e.g. leaf area index-  
12 quantity of leaves) and function (e.g. leaf level photosynthetic assimilation capacity - quality of leaves)  
13 independent of the meteorological and environmental conditions that drive  $GEP$ . Based on basic linear  
14 regressions, we demonstrated that MODIS derived biophysical products (e.g. VIs) were a proxy for  
15 ecosystem photosynthetic potential rather than  $GEP$ . We reported statistically significant regressions  
16 between VIs (e.g.  $NDVI_{SZA30}$  and  $EVI_{SZA30}$ ) to long term measures of phenology (e.g.  $LUE$  and  $Pc$ ), in  
17 contrast to ecosystem descriptors subject to short term responses to environmental conditions (e.g.  
18  $GEP_{sat}$  and  $\alpha$ ). Our results should extend to other methods and measures of greenness, including VIs  
19 and chromatic indices from phenocams and in situ spectrometers.

20 We found that the linear regressions between MODIS biophysical products and photosynthetic  
21 potential converged on a single function across very diverse biome types, which implies that these  
22 relationships may persist over very large areas, thus improving our ability to extrapolate in situ  
23 phenology and seasonality to continental scales, across longer temporal scales and to identify rapid

1 changes due to extreme events or spatial variations at ecotones. We further found that saturation of  
2  $fPAR_{MOD}$  and  $NDVI_{SZA30}$ , restricted their usefulness, except in comparatively low biomass ecosystems  
3 (savannas and arid and semi-arid savannas and woodlands).

4 We quantified how much of  $GEP$  seasonality could be explained by different variables: radiation  
5 ( $SW_{down}$ ), temperature ( $T_{air}$ ), precipitation ( $Precip$ ), or phenology ( $VIs$  as proxy). Our analysis showed  
6 the relationship between RS products and  $GEP$  was only clear when productivity was driven by either:  
7 (1) ecosystem phenology and climate, synchronously driving  $GEP$ , as was observed at Alice Springs  
8 Mulga woodland (AU-ASM), and similar to many temperate deciduous locations, or (2) solely by the  
9 vegetation photosynthetic potential, as observed at the tropical savanna site of Howard Springs (AU-  
10 How). At AU-How, radiation and temperature were constant across the year, although ecosystem  
11 photosynthetic activity ( $GEP$ ) and potential (e.g.  $Pc$  and  $LUE$ ) fluctuated with the highly seasonal  
12 understory. However, RS products do not follow  $GEP$  when: (3) phenology is asynchronous with key  
13 meteorological drivers such that  $GEP$  is driven by one or the other at different times of the year, as we  
14 observed at AU-Cpr; or when (4)  $GEP$  is driven by meteorology ( $SW_{down}$ ,  $T_{air}$ , soil water availability,  
15  $VPD$ , or different combinations) and photosynthetic potential is aseasonal, as observed at AU-Tum. At  
16 AU-Tum, changes in productivity were driven by  $SW_{down}$ , while the ecosystem biophysical properties  
17 remained relatively constant across the year, represented by the small amplitude of the annual cycles in  
18  $Pc$  and  $LUE$  (true evergreen forest). An understanding of why satellite *versus* flux tower estimates of  
19  $GEP$  relationships hold, or do not hold, greatly contribute to our comprehension of carbon cycle  
20 mechanisms and scaling factors at play (e.g. climate and phenology, among others).

## 21 **Acknowledgements**

22 This work was supported by an Australian Research Council Discovery Research Grant (ARC  
23 DP110105479) “Integrating remote sensing, landscape flux measurements, and phenology to

1 understand the impacts of climate change on Australian landscapes and the Australian Government's  
2 Terrestrial Ecosystems Research Network". TERN ([www.tern.gov.au](http://www.tern.gov.au)) is a research infrastructure  
3 facility established under the National Collaborative Research Infrastructure Strategy and Education  
4 Infrastructure Fund (Super Science Initiative) through the Department of Industry, Innovation, Science,  
5 Research and Tertiary Education. We utilized data collected by grants funded by the Australian  
6 Research Council (DP0344744, DP0772981 and DP130101566). J. Beringer is funded under an  
7 Australian Research Council Future Fellowship (ARC FT110100602).

8 The authors would like to thank our collaborators Professor Scott R. Saleska, Dr. Sabina Belli, and Dr.  
9 Piyachat Ratana. Special acknowledgement to Tim Lubcke, Rolf Faux, and Dr. Nicole Grant for  
10 technical support at different OzFlux sites. We acknowledge the contributions of Dr. Georg Wohlfahrt  
11 and two anonymous Reviewers whose comments helped us to improve the clarity and scientific rigour  
12 of this manuscript.

13 We show our respect and acknowledge the people, the traditional custodians of the Land, of Elders past  
14 and present of the Arrernte Nation at Alice Springs, the Wiradjuri people at Tumbarumba, the Meru  
15 people at Calperum-Chowilla and the Woolna nation at Howard Springs.

## 16 **References**

Ainsworth, E. A. and Long, S. P.: What have we learned from 15 years of free-air CO<sub>2</sub> enrichment (FACE)? A meta-analytic review of the responses of photosynthesis, canopy properties and plant production to rising CO<sub>2</sub>, *New Phytol.*, 165(2), 351–371, doi:10.1111/j.1469-8137.2004.01224.x, 2005.

Baldocchi, D.: Measuring fluxes of trace gases and energy between ecosystems and the atmosphere – the state and future of the eddy covariance method, *Glob. Change Biol.*, 20(12), 3600–3609,

doi:10.1111/gcb.12649, 2014.

Baldocchi, D., Falge, E., Gu, L., Olson, R., Hollinger, D., Running, S., Anthoni, P., Bernhofer, C., Davis, K., Evans, R., Fuentes, J., Goldstein, A., Katul, G., Law, B., Lee, X., Malhi, Y., Meyers, T., Munger, W., Oechel, W., Paw, K. T., Pilegaard, K., Schmid, H. P., Valentini, R., Verma, S., Vesala, T., Wilson, K. and Wofsy, S.: FLUXNET: A New Tool to Study the Temporal and Spatial Variability of Ecosystem-Scale Carbon Dioxide, Water Vapor, and Energy Flux Densities, *Bull. Am. Meteorol. Soc.*, 82(11), 2415–2434, doi:10.1175/1520-0477(2001)082<2415:FANTTS>2.3.CO;2, 2001.

Baldocchi, D. D.: Assessing the eddy covariance technique for evaluating carbon dioxide exchange rates of ecosystems: past, present and future, *Glob. Change Biol.*, 9(4), 479–492, doi:10.1046/j.1365-2486.2003.00629.x, 2003.

Balzarolo, M., Vescovo, L., Hammerle, A., Gianelle, D., Papale, D., Tomelleri, E. and Wohlfahrt, G.: On the relationship between ecosystem-scale hyperspectral reflectance and CO<sub>2</sub> exchange in European mountain grasslands, *Biogeosciences*, 12(10), 3089–3108, doi:10.5194/bg-12-3089-2015, 2015.

Barr, A., Hollinger, D. Y. and Richardson, A. D.: CO<sub>2</sub> Flux Measurement Uncertainty Estimates for NACP, 2009.

Beringer, J., Hutley, L. B., Tapper, N. J. and Cernusak, L. A.: Savanna fires and their impact on net ecosystem productivity in North Australia, *Glob. Change Biol.*, 13(5), 990–1004, doi:10.1111/j.1365-2486.2007.01334.x, 2007.

Beringer, J., Hutley, L. B., McHugh, I., Arndt, S. K., Campbell, D., Cleugh, H. A., Cleverly, J., Resco de Dios, V., Eamus, D., Evans, B., Ewenz, C., Grace, P., Griebel, A., Haverd, V., Hinko-Najera, N., Huete, A., Isaac, P., Kanniah, K., Leuning, R., Liddell, M. J., Macfarlane, C., Meyer, W., Moore, C., Pendall, E., Phillips, A., Phillips, R. L., Prober, S., Restrepo-Coupe, N., Rutledge, S., Schroder, I.,

Silberstein, R., Southall, P., Sun, M., Tapper, N. J., van Gorsel, E., Vote, C., Walker, J. and Wardlaw, T.: An introduction to the Australian and New Zealand flux tower network &ndash; OzFlux, *Biogeosciences Discuss.*, 1–52, doi:10.5194/bg-2016-152, 2016.

BOM: Special Climate Statement 41 - Extreme November heat in eastern Australia, Australian Bureau of Meteorology, Melbourne, Australia., 2012.

BOM: Special Climate Statement 45 - a prolonged autumn heatwave for southeast Australia, Australian Bureau of Meteorology, Melbourne, Australia., 2013.

Case, J. L., LaFontaine, F. J., Bell, J. R., Jedlovec, G. J., Kumar, S. V. and Peters-Lidard, C. D.: A Real-Time MODIS Vegetation Product for Land Surface and Numerical Weather Prediction Models, *IEEE Trans. Geosci. Remote Sens.*, 52(3), 1772–1786, doi:10.1109/TGRS.2013.2255059, 2014.

Cleverly, J., Boulain, N., Villalobos-Vega, R., Grant, N., Faux, R., Wood, C., Cook, P. G., Yu, Q., Leigh, A. and Eamus, D.: Dynamics of component carbon fluxes in a semi-arid Acacia woodland, central Australia, *J. Geophys. Res. Biogeosciences*, 118(3), 1168–1185, doi:10.1002/jgrg.20101, 2013.

Cleverly, J., Eamus, D., Van Gorsel, E., Chen, C., Rumman, R., Luo, Q., Coupe, N. R., Li, L., Kljun, N., Faux, R., Yu, Q. and Huete, A.: Productivity and evapotranspiration of two contrasting semiarid ecosystems following the 2011 global carbon land sink anomaly, *Agric. For. Meteorol.*, 220, 151–159, doi:10.1016/j.agrformet.2016.01.086, 2016a.

Cleverly, J., Eamus, D., Restrepo Coupe, N., Chen, C., Maes, W., Li, L., Faux, R., Santini, N. S., Rumman, R., Yu, Q. and Huete, A.: Soil moisture controls on phenology and productivity in a semi-arid critical zone, *Sci. Total Environ.*, doi:10.1016/j.scitotenv.2016.05.142, 2016b.

Collatz, G. J., Ball, J. T., Grivet, C. and Berry, J. A.: Physiological and environmental regulation of stomatal conductance, photosynthesis and transpiration: a model that includes a laminar boundary

layer, *Agric. For. Meteorol.*, 54(2–4), 107–136, doi:10.1016/0168-1923(91)90002-8, 1991.

Delpierre, N., Vitasse, Y., Chuine, I., Guillemot, J., Bazot, S., Rutishauser, T. and Rathgeber, C. B. K.: Temperate and boreal forest tree phenology: from organ-scale processes to terrestrial ecosystem models, *Ann. For. Sci.*, 73(1), 5–25, doi:10.1007/s13595-015-0477-6, 2015.

Doughty, C. E., Malhi, Y., Araujo-Murakami, A., Metcalfe, D. B., Silva-Espejo, J. E., Arroyo, L., Heredia, J. P., Pardo-Toledo, E., Mendizabal, L. M., Rojas-Landivar, V. D., Vega-Martinez, M., Flores-Valencia, M., Sibling-Rivero, R., Moreno-Vare, L., Viscarra, L. J., Chuviru-Castro, T., Osinaga-Becerra, M. and Ledezma, R.: Allocation trade-offs dominate the response of tropical forest growth to seasonal and interannual drought, *Ecology*, 95(8), 2192–2201, doi:10.1890/13-1507.1, 2014.

Eamus, D., Hatton, T., Cook, P. and Colvin, C.: *Ecohydrology: : vegetation function, water and resource management*, CSIRO Publishing, Collingwood VIC 3066., 2006.

Eamus, D., Cleverly, J., Boulain, N., Grant, N., Faux, R. and Villalobos-Vega, R.: Carbon and water fluxes in an arid-zone Acacia savanna woodland: An analyses of seasonal patterns and responses to rainfall events, *Agric. For. Meteorol.*, 182–183(3–4), 225–238, doi:10.1016/j.agrformet.2013.04.020, 2013.

Ehleringer, J. R., Cerling, T. E. and Helliker, B. R.: C4 photosynthesis, atmospheric CO<sub>2</sub>, and climate, *Oecologia*, 112, 285–299, 1997.

Falge, E., Baldocchi, D., Olson, R., Anthoni, P., Aubinet, M., Bernhofer, C., Burba, G., Ceulemans, R., Clement, R., Dolman, H. and others: Gap filling strategies for defensible annual sums of net ecosystem exchange, *Agric. For. Meteorol.*, 107(1), 43–69, 2001.

Fasullo, J. T., Boening, C., Landerer, F. W. and Nerem, R. S.: Australia's unique influence on global sea level in 2010–2011, *Geophys. Res. Lett.*, 40(16), 4368–4373, doi:10.1002/grl.50834, 2013.

Fatichi, S., Leuzinger, S. and Körner, C.: Moving beyond photosynthesis: from carbon source to sink-driven vegetation modeling, *New Phytol.*, 201(4), 1086–1095, doi:10.1111/nph.12614, 2014.

Gamon, J. A., Huemmrich, K. F., Stone, R. S. and Tweedie, C. E.: Spatial and temporal variation in primary productivity (NDVI) of coastal Alaskan tundra: Decreased vegetation growth following earlier snowmelt, *Remote Sens. Environ.*, 129, 144–153, doi:10.1016/j.rse.2012.10.030, 2013.

Gao, X., Huete, A. R., Ni, W. and Miura, T.: Optical–Biophysical Relationships of Vegetation Spectra without Background Contamination, *Remote Sens. Environ.*, 74(3), 609–620, doi:10.1016/S0034-4257(00)00150-4, 2000.

Gesch, D. B., Verdin, K. L. and Greenlee, S. K.: New land surface digital elevation model covers the Earth, *Eos Trans. Am. Geophys. Union*, 80(6), 69–70, doi:10.1029/99EO00050, 1999.

van Gorsel, E., Wolf, S., Isaac, P., Cleverly, J., Haverd, V., Ewenz, C., Arndt, S., Beringer, J., Resco de Dios, V., Evans, B. J., Griebel, A., Hutley, L. B., Keenan, T., Kljun, N., Macfarlane, C., Meyer, W. S., McHugh, I., Pendall, E., Prober, S. and Silberstein, R.: Carbon uptake and water use in woodlands and forests in southern Australia during an extreme heat wave event in the “Angry Summer” of 2012/2013, *Biogeosciences Discuss.*, 1–31, doi:10.5194/bg-2016-183, 2016.

Hill, M. J., Held, A. A., Leuning, R., Coops, N. C., Hughes, D. and Cleugh, H. A.: MODIS spectral signals at a flux tower site: Relationships with high-resolution data, and CO<sub>2</sub> flux and light use efficiency measurements, *Remote Sens. Environ.*, 103(3), 351–368, doi:10.1016/j.rse.2005.06.015, 2006.

Huete, A., Justice, C. and Liu, H.: Development of vegetation and soil indices for MODIS-EOS, *Remote Sens. Environ.*, 49(3), 224–234, doi:10.1016/0034-4257(94)90018-3, 1994.

Huete, A., Didan, K., Miura, T., Rodriguez, E. P., Gao, X. and Ferreira, L. G.: Overview of the

radiometric and biophysical performance of the MODIS vegetation indices, *Remote Sens. Environ.*, 83(1–2), 195–213, doi:10.1016/S0034-4257(02)00096-2, 2002.

Huete, A., Restrepo-Coupe, N., Ratana, P., Didan, K., Saleska, S., Ichii, K., Panuthai, S. and Gamo, M.: Multiple site tower flux and remote sensing comparisons of tropical forest dynamics in Monsoon Asia, *Agric. For. Meteorol.*, 148(5), 748–760, doi:10.1016/j.agrformet.2008.01.012, 2008.

Huete, A. R.: A soil-adjusted vegetation index (SAVI), *Remote Sens. Environ.*, 25(3), 295–309, doi:10.1016/0034-4257(88)90106-X, 1988.

Huete, A. R. and Tucker, C. J.: Investigation of soil influences in AVHRR red and near-infrared vegetation index imagery, *Int. J. Remote Sens.*, 12(6), 1223–1242, doi:10.1080/01431169108929723, 1991.

Huete, A. R., Didan, K., Shimabukuro, Y. E., Ratana, P., Saleska, S. R., Hutyra, L. R., Yang, W., Nemani, R. R. and Myneni, R.: Amazon rainforests green-up with sunlight in dry season, *Geophys. Res. Lett.*, 33, L06405, doi:200610.1029/2005GL025583, 2006.

Huffman, G. J., Bolvin, D. T., Nelkin, E. J., Wolff, D. B., Adler, R. F., Gu, G., Hong, Y., Bowman, K. P. and Stocker, E. F.: The TRMM Multisatellite Precipitation Analysis (TMPA): Quasi-Global, Multiyear, Combined-Sensor Precipitation Estimates at Fine Scales, *J. Hydrometeorol.*, 8(1), 38–55, doi:10.1175/JHM560.1, 2007.

Hutley, L. B., O’Grady, A. P. and Eamus, D.: Evapotranspiration from Eucalypt open-forest savanna of Northern Australia, *Funct. Ecol.*, 14(2), 183–194, doi:10.1046/j.1365-2435.2000.00416.x, 2000.

Hutley, L. B., Beringer, J., Isaac, P. R., Hacker, J. M. and Cernusak, L. A.: A sub-continental scale living laboratory: Spatial patterns of savanna vegetation over a rainfall gradient in northern Australia, *Agric. For. Meteorol.*, 151(11), 1417–1428, doi:10.1016/j.agrformet.2011.03.002, 2011.



Hutyra, L. R., Munger, J. W., Saleska, S. R., Gottlieb, E., Daube, B. C., Dunn, A. L., Amaral, D. F., de Camargo, P. B. and Wofsy, S. C.: Seasonal controls on the exchange of carbon and water in an Amazonian rain forest, *J. Geophys. Res. Biogeosciences*, 112(G3), 1–16, doi:10.1029/2006JG000365, 2007.

Isaac, P., Cleverly, J., McHugh, I., van Gorsel, E., Ewenz, C. and Beringer, J.: OzFlux Data: Network integration from collection to curation, *Biogeosciences Discuss.*, 1–41, doi:10.5194/bg-2016-189, 2016.

Johnson, K. A. and Goody, R. S.: The Original Michaelis Constant: Translation of the 1913 Michaelis–Menten Paper, *Biochemistry (Mosc.)*, 50(39), 8264–8269, doi:10.1021/bi201284u, 2011.

Jurik, T. W.: Seasonal Patterns of Leaf Photosynthetic Capacity in Successional Northern Hardwood Tree Species, *Am. J. Bot.*, 73(1), 131–138, 1986.

Kanniah, K. D., Beringer, J., Hutley, L. B., Tapper, N. J. and Zhu, X.: Evaluation of Collections 4 and 5 of the MODIS Gross Primary Productivity product and algorithm improvement at a tropical savanna site in northern Australia, *Remote Sens. Environ.*, 113(9), 1808–1822, doi:10.1016/j.rse.2009.04.013, 2009.

Kanniah, K. D., Beringer, J. and Hutley, L. B.: Environmental controls on the spatial variability of savanna productivity in the Northern Territory, Australia, *Savanna Patterns Energy Carbon Integr. Landsc. Spec.*, 151(11), 1429–1439, doi:10.1016/j.agrformet.2011.06.009, 2011.

Kanniah, K. D., Beringer, J., North, P. and Hutley, L.: Control of atmospheric particles on diffuse radiation and terrestrial plant productivity A review, *Prog. Phys. Geogr.*, 36(2), 209–237, doi:10.1177/0309133311434244, 2012.

Kanniah, K. D., Beringer, J. and Hutley, L.: Exploring the link between clouds, radiation, and canopy

productivity of tropical savannas, *Agric. For. Meteorol.*, 182–183, 304–313, doi:10.1016/j.agrformet.2013.06.010, 2013.

Kato, S., Loeb, N. G., Rose, F. G., Doelling, D. R., Rutan, D. A., Caldwell, T. E., Yu, L. and Weller, R. A.: Surface Irradiances Consistent with CERES-Derived Top-of-Atmosphere Shortwave and Longwave Irradiances, *J. Clim.*, 26(9), 2719–2740, doi:10.1175/JCLI-D-12-00436.1, 2012.

Knyazikhin, Y., Glassy, J., Privette, J. L., Tian, Y., Lotsch, A., Zhang, Y., Wang, Y., Morisette, J. T., Votava, P., Myneni, R. B., Nemani, R. R. and Running, S. W.: MODIS Leaf Area Index (LAI) and Fraction of Photosynthetically Active Radiation Absorbed by Vegetation (FPAR) Product (MOD15): Algorithm Theoretical Basis Document, [online] Available from: [http://modis.gsfc.nasa.gov/data/atbd/atbd\\_mod15.pdf](http://modis.gsfc.nasa.gov/data/atbd/atbd_mod15.pdf) (Accessed 20 December 2012), 1999.

Koerber, G. R., Meyer, W. S., Sun, Q., Cale, P. and Ewenz, C. M.: Under a new light: validation of eddy covariance flux with light response functions of assimilation and estimates of heterotrophic soil respiration, *Biogeosciences Discuss.*, 1–28, doi:10.5194/bg-2016-182, 2016.

Kottek, M., Grieser, J., Beck, C., Rudolf, B. and Rubel, F.: World Map of the Köppen-Geiger climate classification updated, *Meteorol. Z.*, 15(3), 259–263, doi:10.1127/0941-2948/2006/0130, 2006.

Leuning, R., Cleugh, H. A., Zegelin, S. J. and Hughes, D.: Carbon and water fluxes over a temperate Eucalyptus forest and a tropical wet/dry savanna in Australia: measurements and comparison with MODIS remote sensing estimates, *Agric. For. Meteorol.*, 129(3–4), 151–173, doi:10.1016/j.agrformet.2004.12.004, 2005.

Ma, X., Huete, A., Yu, Q., Coupe, N. R., Davies, K., Broich, M., Ratana, P., Beringer, J., Hutley, L. B., Cleverly, J., Boulain, N. and Eamus, D.: Spatial patterns and temporal dynamics in savanna vegetation phenology across the North Australian Tropical Transect, *Remote Sens. Environ.*, 139(0), 97–115,

doi:10.1016/j.rse.2013.07.030, 2013.

Ma, X., Huete, A., Yu, Q., Restrepo-Coupe, N., Beringer, J., Hutley, L. B., Kanniah, K. D., Cleverly, J. and Eamus, D.: Parameterization of an ecosystem light-use-efficiency model for predicting savanna GPP using MODIS EVI, *Remote Sens. Environ.*, 154, 253–271, doi:10.1016/j.rse.2014.08.025, 2014.

Maeda, E. E., Heiskanen, J., Aragão, L. E. O. C. and Rinne, J.: Can MODIS EVI monitor ecosystem productivity in the Amazon rainforest?, *Geophys. Res. Lett.*, 41(20), 2014GL061535, doi:10.1002/2014GL061535, 2014.

Mahadevan, P., Wofsy, S. C., Matross, D. M., Xiao, X., Dunn, A. L., Lin, J. C., Gerbig, C., Munger, J. W., Chow, V. Y. and Gottlieb, E. W.: A satellite-based biosphere parameterization for net ecosystem CO<sub>2</sub> exchange: Vegetation Photosynthesis and Respiration Model (VPRM), *Glob. Biogeochem. Cycles*, 22(2), B2005, doi:10.1029/2006GB002735, 2008.

Meyer, W. S., Kondrlovà, E. and Koerber, G. R.: Evaporation of perennial semi-arid woodland in southeastern Australia is adapted for irregular but common dry periods, *Hydrol. Process.*, 29(17), 3714–3726, doi:10.1002/hyp.10467, 2015.

Michaelis, L. and Menten, M. L.: Die Kinetik der Invertinwirkung, *Biochemistry (Mosc.)*, 49, 333–369, 1913.

NASA: Clouds and the Earth's Radiant Energy System Information and Data (CERES), [online] Available from: <http://ceres.larc.nasa.gov/> (Accessed 28 August 2015a), 2014.

NASA: Tropical Rainfall Measuring Mission Project (TRMM), 3B43: Monthly 0.25x0.25 degree merged TRMM and other estimates v7, NASA Distrib Act. Arch Cent Goddard Space Flight Cent Earth Sci Greenbelt Md [online] Available from: <http://mirador.gsfc.nasa.gov/cgi-bin/mirador/> (Accessed 27 February 2016b), 2014.

van Niel, T. G., McVicar, T. R., Roderick, M. L., van Dijk, A. I. J. M., Beringer, J., Hutley, L. B. and van Gorsel, E.: Upscaling latent heat flux for thermal remote sensing studies: Comparison of alternative approaches and correction of bias, *J. Hydrol.*, 468–469, 35–46, doi:10.1016/j.jhydrol.2012.08.005, 2012.

Olofsson, P., Lagergren, F., Lindroth, A., Lindström, J., Klemedtsson, L., Kutsch, W. and Eklundh, L.: Towards operational remote sensing of forest carbon balance across Northern Europe, *Biogeosciences*, 5(3), 817–832, doi:10.5194/bg-5-817-2008, 2008.

Papaioannou, G., Papanikolaou, N. and Retalis, D.: Relationships of photosynthetically active radiation and shortwave irradiance, *Theor. Appl. Climatol.*, 48(1), 23–27, doi:10.1007/BF00864910, 1993.

Papale, D., Reichstein, M., Aubinet, M., Canfora, E., Bernhofer, C., Kutsch, W., Longdoz, B., Rambal, S., Valentini, R., Vesala, T. and Yakir, D.: Towards a standardized processing of Net Ecosystem Exchange measured with eddy covariance technique: Algorithms and uncertainty estimation, *Biogeosciences*, 3(4), 571–583, 2006.

Peng, Y. and Gitelson, A. A.: Remote estimation of gross primary productivity in soybean and maize based on total crop chlorophyll content, *Remote Sens. Environ.*, 117, 440–448, doi:10.1016/j.rse.2011.10.021, 2012.

Poulter, B., Frank, D., Ciais, P., Myneni, R. B., Andela, N., Bi, J., Broquet, G., Canadell, J. G., Chevallier, F., Liu, Y. Y., Running, S. W., Sitch, S. and van der Werf, G. R.: Contribution of semi-arid ecosystems to interannual variability of the global carbon cycle, *Nature*, 509(7502), 600–603, doi:10.1038/nature13376, 2014.

Restrepo Coupe, N., Huete, A. R. and Davis, K.: Satellite Phenology Validation, in *AusCover Good Practice Guidelines: A technical handbook supporting calibration and validation activities of remotely*

sensed data products, TERN, Canberra, ATC, Australia., 2015.

Restrepo-Coupe, N., da Rocha, H. R., da Araujo, A. C., Borma, L. S., Christoffersen, B., Cabral, O. M. R., de Camargo, P. B., Cardoso, F. L., da Costa, A. C. L., Fitzjarrald, D. R., Goulden, M. L., Kruijt, B., Maia, J. M. F., Malhi, Y. S., Manzi, A. O., Miller, S. D., Nobre, A. D., von Randow, C., Sá, L. D. A., Sakai, R. K., Tota, J., Wofsy, S. C., Zanchi, F. B. and Saleska, S. R.: What drives the seasonality of photosynthesis across the Amazon basin? A cross-site analysis of eddy flux tower measurements from the Brasil flux network, *Agric. For. Meteorol.*, 182–183, 128–144, 2013.

Richardson, A. D. and Hollinger, D. Y.: Statistical modeling of ecosystem respiration using eddy covariance data: Maximum likelihood parameter estimation, and Monte Carlo simulation of model and parameter uncertainty, applied to three simple models, *Agric. For. Meteorol.*, 131(3–4), 191–208, doi:10.1016/j.agrformet.2005.05.008, 2005.

Rubel, F. and Kottek, M.: Observed and projected climate shifts 1901–2100 depicted by world maps of the Köppen-Geiger climate classification, *Meteorol. Z.*, 19(2), 135–141, doi:10.1127/0941-2948/2010/0430, 2010.

Running, S. W., Justice, C. O., Salomonson, V., Hall, D., Barker, J., Kaufmann, Y. J., Strahler, A. H., Huete, A. R., Muller, J.-P., Vanderbilt, V., Wan, Z. M., Teillet, P. and Carneggie, D.: Terrestrial remote sensing science and algorithms planned for EOS/MODIS, *Int. J. Remote Sens.*, 15(17), 3587–3620, doi:10.1080/01431169408954346, 1994.

Running, S. W., Thornton, P. E., Nemani, R. and Glassy, J. M.: Global terrestrial gross and net primary productivity from the Earth Observing System, in *Methods in ecosystem science*, pp. 44–57, Springer, New York., 2000.

Santin-Janin, H., Garel, M., Chapuis, J.-L. and Pontier, D.: Assessing the performance of NDVI as a

proxy for plant biomass using non-linear models: a case study on the Kerguelen archipelago, *Polar Biol.*, 32(6), 861–871, doi:10.1007/s00300-009-0586-5, 2009.

Schaaf, C. B., Gao, F., Strahler, A. H., Lucht, W., Li, X., Tsang, T., Strugnell, N. C., Zhang, X., Jin, Y., Muller, J.-P., Lewis, P., Barnsley, M., Hobson, P., Disney, M., Roberts, G., Dunderdale, M., Doll, C., d'Entremont, R. P., Hu, B., Liang, S., Privette, J. L. and Roy, D.: First operational BRDF, albedo nadir reflectance products from MODIS, *Remote Sens. Environ.*, 83(1–2), 135–148, doi:10.1016/S0034-4257(02)00091-3, 2002.

Shen, S. and Leptoukh, G. G.: Estimation of surface air temperature over central and eastern Eurasia from MODIS land surface temperature, *Environ. Res. Lett.*, 6(4), 45206, doi:10.1088/1748-9326/6/4/045206, 2011.

Shi, H., Li, L., Eamus, D., Cleverly, J., Huete, A., Beringer, J., Yu, Q., Gorsel, E. van and Hutley, L.: Intrinsic climate dependency of ecosystem light and water-use-efficiencies across Australian biomes, *Environ. Res. Lett.*, 9(10), 104002, doi:10.1088/1748-9326/9/10/104002, 2014.

Sims, D. A., Rahman, A. F., Cordova, V. D., El-Masri, B. Z., Baldocchi, D. D., Flanagan, L. B., Goldstein, A. H., Hollinger, D. Y., Misson, L., Monson, R. K., Oechel, W. C., Schmid, H. P., Wofsy, S. C. and Xu, L.: On the use of MODIS EVI to assess gross primary productivity of North American ecosystems, *J. Geophys. Res. Biogeosciences*, 111(G4), G04015, doi:10.1029/2006JG000162, 2006.

Sims, D. A., Rahman, A. F., Cordova, V. D., El-Masri, B. Z., Baldocchi, D. D., Bolstad, P. V., Flanagan, L. B., Goldstein, A. H., Hollinger, D. Y., Misson, L., Monson, R. K., Oechel, W. C., Schmid, H. P., Wofsy, S. C. and Xu, L.: A new model of gross primary productivity for North American ecosystems based solely on the enhanced vegetation index and land surface temperature from MODIS, *Remote Sens. Data Assim. Spec. Issue*, 112(4), 1633–1646, doi:10.1016/j.rse.2007.08.004, 2008.

Sjöström, M., Ardö, J., Arneth, A., Boulain, N., Cappelaere, B., Eklundh, L., de Grandcourt, A., Kutsch, W. L., Merbold, L., Nouvellon, Y., Scholes, R. J., Schubert, P., Seaquist, J. and Veenendaal, E. M.: Exploring the potential of MODIS EVI for modeling gross primary production across African ecosystems, *Remote Sens. Environ.*, 115(4), 1081–1089, doi:10.1016/j.rse.2010.12.013, 2011.

Stoy, P. C., Katul, G. G., Siqueira, M. B. S., Juang, J.-Y., Novick, K. A., Uebelherr, J. M. and Oren, R.: An evaluation of models for partitioning eddy covariance-measured net ecosystem exchange into photosynthesis and respiration, *Agric. For. Meteorol.*, 141(1), 2–18, doi:doi: DOI: 10.1016/j.agrformet.2006.09.001, 2006.

Suyker, A. E. and Verma, S. B.: Year-round observations of the net ecosystem exchange of carbon dioxide in a native tallgrass prairie, *Glob. Change Biol.*, 7(3), 279–289, doi:10.1046/j.1365-2486.2001.00407.x, 2001.

Szeicz, G.: Solar Radiation for Plant Growth, *J. Appl. Ecol.*, 11(2), 617–636, 1974.

Taylor, K. E.: Summarizing multiple aspects of model performance in a single diagram, *J. Geophys. Res.*, 106(D7), PP. 7183-7192, doi:200110.1029/2000JD900719, 2001.

Tezara, W., Mitchell, V. J., Driscoll, S. D. and Lawlor, D. W.: Water stress inhibits plant photosynthesis by decreasing coupling factor and ATP, *Nature*, 401(6756), 914–917, doi:10.1038/44842, 1999.

Varone, L. and Gratani, L.: Leaf expansion in *Rhamnus alaternus* L. by leaf morphological, anatomical and physiological analysis, *Trees*, 23(6), 1255–1262, doi:10.1007/s00468-009-0365-5, 2009.

Veroustraete, F., Sabbe, H. and Eerens, H.: Estimation of carbon mass fluxes over Europe using the C-Fix model and Euroflux data, *Remote Sens. Environ.*, 83(3), 376–399, doi:10.1016/S0034-4257(02)00043-3, 2002.

Vitasse, Y., Lenz, A. and Körner, C.: The interaction between freezing tolerance and phenology in temperate deciduous trees, *Front. Plant Sci.*, 5, 541, doi:10.3389/fpls.2014.00541, 2014.

Wang, J., Rich, P. M., Price, K. P. and Kettle, W. D.: Relations between NDVI and tree productivity in the central Great Plains, *Int. J. Remote Sens.*, 25(16), 3127–3138, doi:10.1080/0143116032000160499, 2004.

Wofsy, S., Goulden, M. and Munger, J. W.: Net Exchange of CO<sub>2</sub> in a Mid-Latitude Forest, *Science*, 260, 1314–1317, 1993.

Wohlfahrt, G. and Gu, L.: The many meanings of gross photosynthesis and their implication for photosynthesis research from leaf to globe, *Plant Cell Environ.*, 38(12), 2500–2507, doi:10.1111/pce.12569, 2015.

Wohlfahrt, G., Piloni, S., Hörtnagl, L. and Hammerle, A.: Estimating carbon dioxide fluxes from temperate mountain grasslands using broad-band vegetation indices, *Biogeosciences*, 7(2), 683–694, doi:10.5194/bg-7-683-2010, 2010.

Wu, C., Niu, Z. and Gao, S.: Gross primary production estimation from MODIS data with vegetation index and photosynthetically active radiation in maize, *J. Geophys. Res. Atmospheres*, 115(D12), D12127, doi:10.1029/2009JD013023, 2010.

Wu, C., Chen, J. M. and Huang, N.: Predicting gross primary production from the enhanced vegetation index and photosynthetically active radiation: Evaluation and calibration, *Remote Sens. Environ.*, 115(12), 3424–3435, doi:10.1016/j.rse.2011.08.006, 2011.

Xiao, X., Zhang, Q., Braswell, B., Urbanski, S., Boles, S., Wofsy, S., Moore III, B. and Ojima, D.: Modeling gross primary production of temperate deciduous broadleaf forest using satellite images and climate data, *Remote Sens. Environ.*, 91(2), 256–270, doi:10.1016/j.rse.2004.03.010, 2004.



Zolfaghar, S.: Comparative ecophysiology of Eucalyptus woodlands along a depth-to-groundwater gradient, PhD thesis, University Technology of Sydney, Sydney, Australia, 1 September., 2013.

## 1 **List of tables**

2 Table 1. OzFlux sites presented in this study -location and additional information.

3 Table 2. Remote sensing data sources, cell size, sample size (eddy-covariance tower-site at the centre  
4 pixel) and time interval.

5 Table 3. Linear regressions obtained by a non-linear mixed-effects regression model for gross  
6 ecosystem productivity ( $GEP$ ,  $\text{gC m}^{-2} \text{d}^{-1}$ ) versus combinations of 16-day average MODIS products:  
7 fixed solar zenith angle of  $30^\circ$  enhanced vegetation index ( $EVI_{\text{SZA}30}$ ), daytime and land surface  
8 temperature ( $LST_{\text{day}}$ ,  $^\circ\text{C}$ ), fixed solar zenith angle of  $30^\circ$  normalized difference vegetation index ( $NDVI$   
9  $\text{SZA}30$ ), precipitation from the Tropical Rainfall Measuring Mission ( $Precip_{\text{TRMM}}$ ,  $\text{mm month}^{-1}$ ) data  
10 product from 1998-2013 (NASA, 2014b), and surface shortwave incident radiation from the Clouds  
11 and the Earth's Radiant Energy System ( $SW_{\text{CERES}}$ ,  $\text{W m}^{-2}$ ) data product from 2000–2013 (NASA,  
12 2014a). Model runs for AU-How: Howard Springs, AU-ASM: Alice Springs Mulga, AU-Cpr:  
13 Calperum-Chowilla, and AU-Tum: Tumbarumba, and all available data (includes all sites). Bold fonts  
14 highlight values mentioned on the text.

## 15 **List of figures**

16 Figure 1. Location of four OzFlux eddy covariance tower sites included on this analysis: AU-How:

1 Howard Springs (at Aw), AU-ASM: Alice Springs Mulga (at BSh and BWh boundary), AU-Cpr:  
2 Calperum-Chowilla (at Bwk), and AU-Tum: Tumberumba (at Cfa and Cfb boundary). Köppen-Geiger  
3 climate classification as published by Kottek et al. (2006) and Rubel and Kottek (2010). Where Aw is  
4 equatorial winter dry climate, BSh is arid steppe, BWh is hot arid desert, Bwk is cold arid desert, Cfb  
5 is warm temperate fully humid warm summer, Cfa is warm temperate fully humid hot summer and  
6 Cwa is warm temperate winter dry hot summer. Other climate classes are: Equatorial fully humid (Af)  
7 and monsoonal climate (Am), arid summer dry and cold desert (Bsk), and warm temperate hot summer  
8 (Csa) and warm summer (Csb) steppes.

9 Figure 2. Rectangular hyperbola fitted to 16-day worth of hourly gross ecosystem productivity ( $GEP$ ,  
10  $\mu\text{molCO}_2 \text{ m}^{-2} \text{ s}^{-1}$ ) versus photosynthetic active radiation ( $PAR$ ,  $\mu\text{mol m}^{-2} \text{ s}^{-1}$ ) data measured at Howard  
11 Springs eddy covariance tower (black line). From the rectangular hyperbola: quantum yield ( $\alpha$ ,  
12  $\mu\text{molCO}_2 \mu\text{mol}^{-1}$ ) (blue dashed line) and  $GEP$  at saturation ( $GEP_{sat}$ ,  $\mu\text{molCO}_2 \text{ m}^{-2} \text{ s}^{-1}$ ) (blue dotted line).  
13 Photosynthetic capacity ( $P_c$ ,  $\mu\text{molCO}_2 \text{ m}^{-2} \text{ s}^{-1}$ ) (black dashed line) was calculated as the 16-day mean  
14  $GEP$  at mean annual daytime  $PAR$  ( $\overline{PAR}$ )  $\pm 100 \mu\text{mol m}^{-2} \text{ s}^{-1}$  (grey area) and mean annual  $VPD$  ( $\overline{VPD}$ )  $\pm 2$   
15 standard deviations. Light use efficiency ( $LUE$ ,  $\mu\text{molCO}_2 \mu\text{mol}^{-1}$ ) was defined as the ratio between  
16 daily  $GEP$  over  $PAR$ , the slope of the linear regression (blue line).

17 Figure 3. Savanna (AU-How), wet sclerophyll (AU-Tum), Mulga (AU-ASM), and Mallee (AU-Cpr)  
18 ecosystems, OzFlux sites annual cycle (16-day composites) of (a) precipitation ( $Precip$ ;  $\text{mm month}^{-1}$ )  
19 (grey bars) and photosynthetic active radiation ( $PAR$ ;  $\mu\text{mol m}^{-2} \text{ d}^{-1}$ ) (blue line), and (b) vapour pressure  
20 deficit ( $VPD$ ;  $\text{kPa}$ ) (black line) and air temperature ( $T_{air}$ ;  $^{\circ}\text{C}$ ) (blue line). Grey boxes indicate Southern  
21 Hemisphere spring and summer September to March.

1 Figure 4. Savanna (AU-How), wet sclerophyll (AU-Tum) , Mulga (AU-ASM), and Mallee (AU-Cpr)  
2 ecosystems, OzFlux sites annual cycle (16-day composites) of eddy flux derived (a) Gross Ecosystem  
3 Productivity ( $GEP$ ;  $\text{gC m}^{-2} \text{d}^{-1}$ ) (black line) and MODIS Gross Primary Productivity ( $GPP_{MOD}$ ) product  
4 (light blue line); (b)  $GEP$  at saturation light ( $GEP_{sat}$ ;  $\text{gC m}^{-2} \text{d}^{-1}$ ) (black line) and ecosystem quantum  
5 yield ( $\alpha$ ;  $\text{gC MJ}^{-1}$ ) (light blue line); (c) photosynthetic capacity ( $Pc$ ;  $\text{gC m}^{-2} \text{d}^{-1}$ ) (black line) and the ratio  
6 of  $GEP$  over  $PAR$  (black line), the light use efficiency ( $LUE$ ;  $\text{gC MJ}^{-1}$ ) (light blue line). At the bottom  
7 two panels, satellite derived data of: (d) MODIS Enhanced Vegetation Index at fixed solar zenith angle  
8 of  $30^\circ$  ( $EVI_{SZA30}$ ) (black line) and the Normalized Difference Vegetation Index ( $NDVI_{SZA30}$ ) (light blue  
9 line); (e) MODIS Leaf Area Index ( $LAI_{MOD}$ ) (black line) and MODIS Fraction of the Absorbed  
10 Photosynthetic Active Radiation ( $fPAR_{MOD}$ ) (light blue line). Grey boxes indicate Southern Hemisphere  
11 spring and summer September to March. Black dashed vertical line indicates the timing of maximum  
12  $GEP$ .

13 Figure 5. Top row: Linear regression between 16 and 8-day time series of measured gross ecosystem  
14 productivity ( $GEP$ ;  $\text{gC m}^{-2} \text{d}^{-1}$ ) (top row) and the MODIS fixed solar zenith angle of  $30^\circ$  enhanced  
15 vegetation index ( $EVI_{SZA30}$ ) at (a) Howard Springs (AU-How) open woodland savanna, (b) Alice  
16 Springs Mulga (AU-ASM), (c) Tumbarumba (AU-Tum) wet sclerophyll forest eddy, and (d) Chowilla  
17 Mallee (AU-Cpr) covariance site. Lower row: Regression between  $GEP$  and MODIS gross primary  
18 productivity ( $GPP_{MOD}$ ) (e) AU-How, (f) AU-Tum, (g) AU-ASM, and (h) AU-Cpr.

19 Figure 6. Relationships between 16-day mean values of (a) light use efficiency ( $LUE$ ;  $\text{gC MJ}^{-1}$ ), (b)  
20 photosynthetic capacity ( $Pc$ ;  $\text{gC m}^{-2} \text{d}^{-1}$ ), (c) ecosystem quantum yield ( $\alpha$ ;  $\text{gC MJ}^{-1}$ ), and (d)  $GEP$  at  
21 saturation light ( $GEP_{sat}$ ;  $\text{gC m}^{-2} \text{d}^{-1}$ ), and MODIS fixed solar zenith angle of  $30^\circ$  enhanced vegetation  
22 index ( $EVI_{SZA30}$ ). Four key Australian ecosystem sites, from left to right (columns), AU-How savanna,  
23 AU-ASM Mulga, wet sclerophyll forest of AU-Tum and AU-Cpr Mallee.

1 Figure 7. Taylor diagrams showing model results for Howard Springs (AU-How), Tumbarumba (AU-  
2 Tum), Alice Springs (AU-ASM) and Calperum-Chowilla (AU-Cpr) based on site-specific and all sites  
3 linear regressions between gross ecosystem productivity (*GEP*), light use efficiency (*LUE*),  
4 photosynthetic capacity (*Pc*) and ecosystem quantum yield ( $\alpha$ ) and different remote sensing products  
5 MODIS fixed solar zenith angle of 30° Enhanced Vegetation Index (*EVI*) and Normalized Difference  
6 Vegetation Index (*NDVI*), Gross Primary Productivity product (*GPP*), daytime Land surface  
7 Temperature (*LST*), Leaf Area Index (*LAI*), fraction of the absorbed Photosynthetic Active Radiation  
8 (*fPAR*). All site relationships is labelled with an asterisk (e.g. *EVI\**). *EVI* and *NDVI* labels are used  
9 instead of *EVI<sub>SZA30</sub>* and *NDVI<sub>SZA30</sub>* for displaying purposes. Missing sites indicate that the model  
10 overestimates the seasonality of observations -model normalized standard deviation is >2.

11 Figure 8. Relationships between 16-day mean values of photosynthetic capacity (*Pc*;  $\text{gC m}^{-2} \text{d}^{-1}$ ) and  
12 different RS products: (a) MODIS fixed solar zenith angle of 30° enhanced vegetation index (*EVI<sub>SZA30</sub>*),  
13 (b) normalized difference vegetation index (*NDVI<sub>SZA30</sub>*), (c) MODIS gross primary productivity  
14 (*GPP<sub>MOD</sub>*;  $\text{gC m}^{-2} \text{d}^{-1}$ ), (d) leaf area index (*LAI<sub>MOD</sub>*), and (e) fraction of the absorbed photosynthetic  
15 active radiation (*fPAR<sub>MOD</sub>*). Four key Australian ecosystem sites included on the analysis: AU-How  
16 savanna (blue circles), AU-ASM Mulga (yellow square markers), AU-Cpr Mallee (red triangles) and  
17 wet sclerophyll forest of AU-Tum (green diamonds).

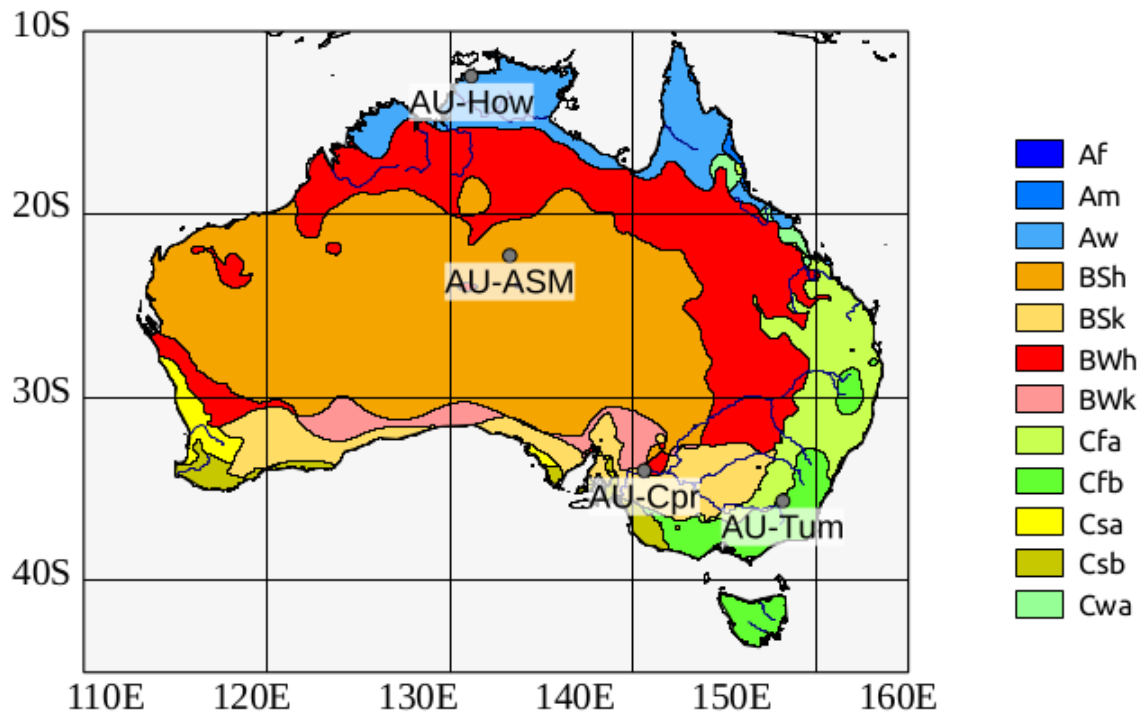


**Figure 1.** Location of four OzFlux eddy covariance tower sites included on this analysis: AU-How: Howard Springs (at Aw), AU-ASM: Alice Springs Mulga (at BSh and BWh boundary), AU-Cpr: Calperum-Chowilla (at BSk and BWk), and AU-Tum: Tumbarumba (at Cfa and Cfb boundary). Köppen-Geiger climate classification as published by Kottek et al. (2006) and Rubel and Kottek (2010). Where Aw is equatorial winter dry climate, BSh is arid steppe, BWh is hot arid desert, BWk is cold arid desert, Cfb is warm temperate fully humid warm summer, Cfa is warm temperate fully humid hot summer and Cwa is warm temperate winter dry hot summer. Other climate classes are: Equatorial fully humid (Af) and monsoonal climate (Am), arid summer dry and cold desert (BSk), and warm temperate hot summer (Csa) and warm summer steppes (Csb).

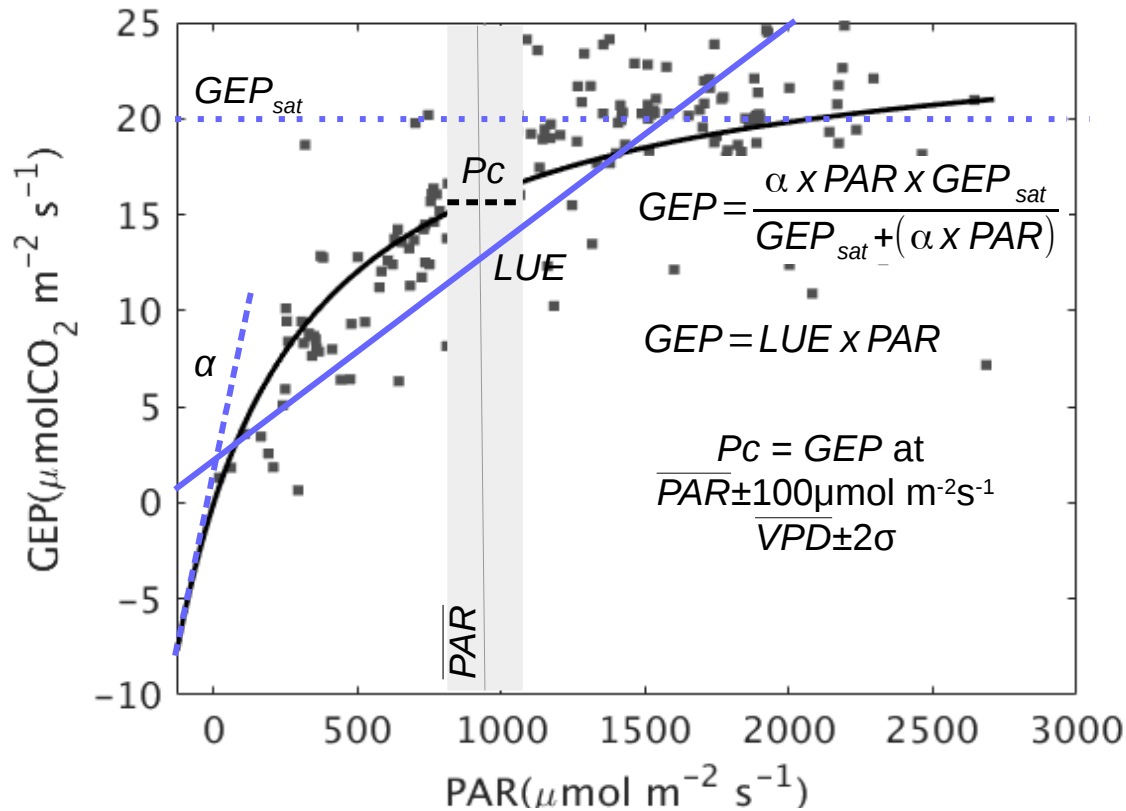


**Figure 2.** Rectangular hyperbola fitted to 16-day worth of hourly gross ecosystem productivity ( $GEP$ ,  $\mu\text{molCO}_2 \text{ m}^{-2} \text{ s}^{-1}$ ) versus photosynthetic active radiation ( $PAR$ ,  $\mu\text{mol m}^{-2} \text{ s}^{-1}$ ) data measured at Howard Springs eddy covariance tower (black line). From the rectangular hyperbola: quantum yield ( $\alpha$ ,  $\mu\text{molCO}_2 \mu\text{mol}^{-1}$ ) (blue dashed line) and  $GEP$  at saturation ( $GEP_{sat}$ ,  $\mu\text{molCO}_2 \text{ m}^{-2} \text{ s}^{-1}$ ) (blue dotted line). Photosynthetic capacity ( $Pc$ ,  $\mu\text{molCO}_2 \text{ m}^{-2} \text{ s}^{-1}$ ) (black dashed line) was calculated as the 16-day mean  $GEP$  at mean annual daytime  $PAR$  ( $\overline{PAR}$ )  $\pm 100 \mu\text{mol m}^{-2} \text{ s}^{-1}$  (grey area) and mean annual  $VPD$  ( $\overline{VPD}$ )  $\pm 2$  standard deviations. Light use efficiency ( $LUE$ ,  $\mu\text{molCO}_2 \mu\text{mol}^{-1}$ ) was defined as the ratio between daily  $GEP$  over  $PAR$ , the slope of the linear regression (blue line).

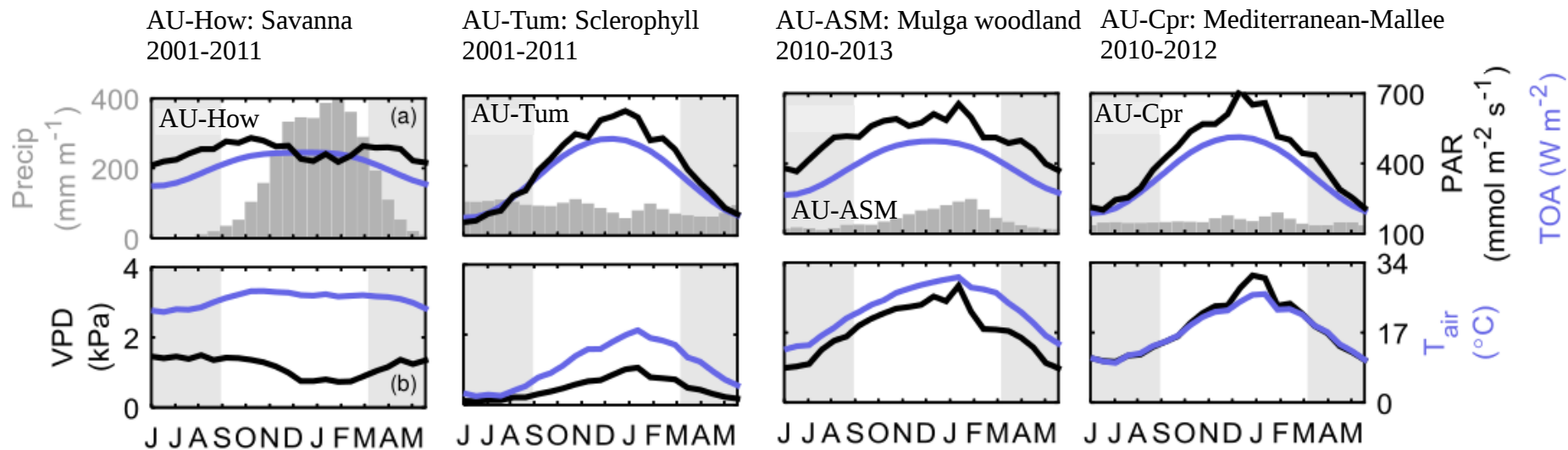


**Figure 3.** Savanna (AU-How), wet sclerophyll (AU-Tum), Mulga (AU-ASM), and Mallee (AU-Cpr) ecosystems, OzFlux sites annual cycle (16-day composites) of (a) precipitation (*Precip*;  $\text{mm month}^{-1}$ ) (grey bars) and photosynthetic active radiation (PAR;  $\mu\text{mol m}^{-2} \text{d}^{-1}$ ) (blue line), and (b) vapour pressure deficit (VPD; kPa) (black line) and air temperature ( $T_{air}$ ;  $^{\circ}\text{C}$ ) (blue line). Grey boxes indicate Southern Hemisphere spring and summer September to March.

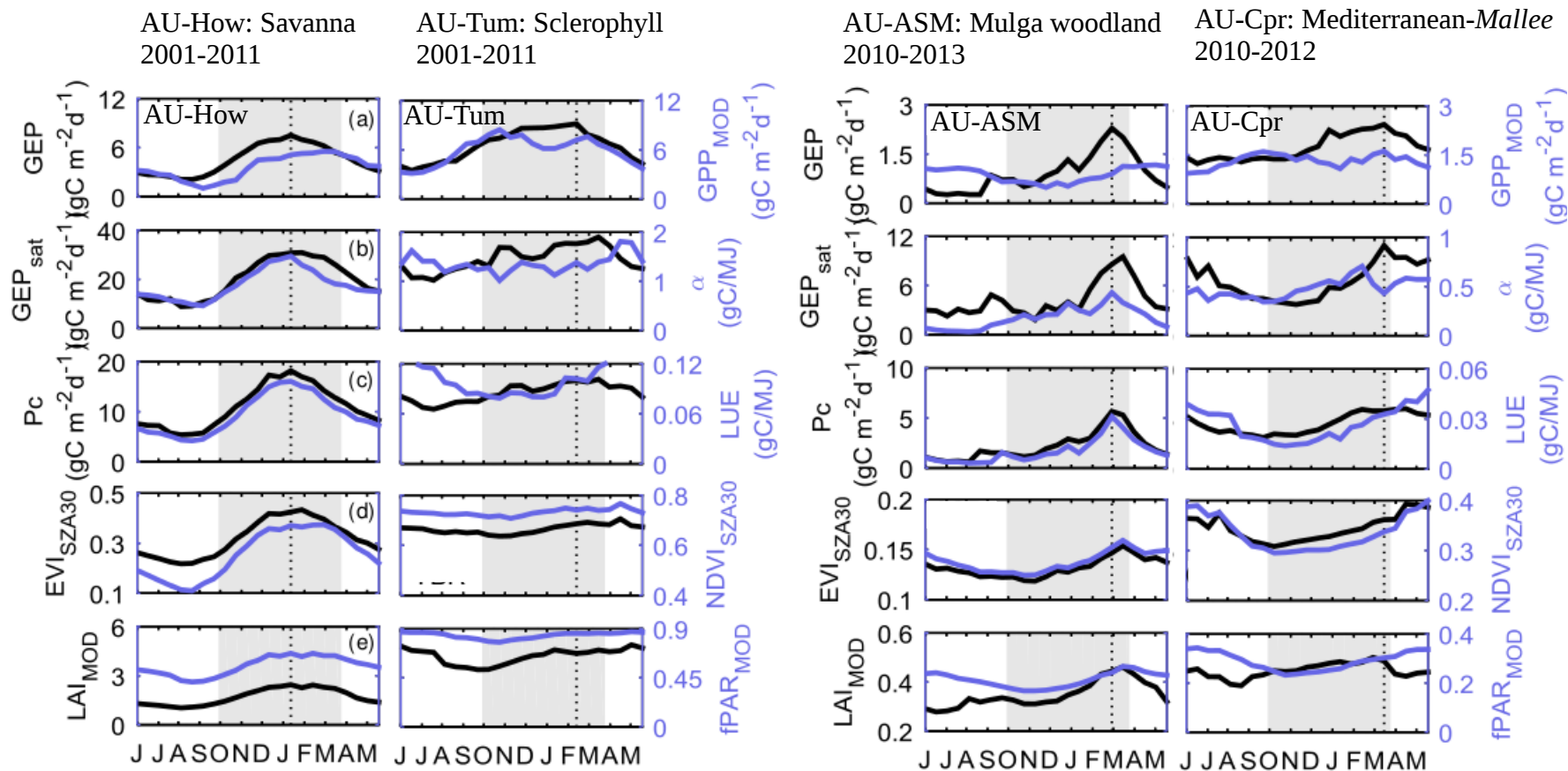


**Figure 4.** Savanna (AU-How), wet sclerophyll (AU-Tum), Mulga (AU-ASM), and Mallee (AU-Cpr) ecosystems, OzFlux sites annual cycle (16-day composites) of eddy flux derived (a) Gross Ecosystem Productivity ( $GEP$ ;  $gC\ m^{-2}\ d^{-1}$ ) (black line) and MODIS Gross Primary Productivity ( $GPP_{MOD}$ ) product (light blue line); (b)  $GEP$  at saturation light ( $GEP_{sat}$ ;  $gC\ m^{-2}\ d^{-1}$ ) (black line) and ecosystem quantum yield ( $\alpha$ ;  $gC\ MJ^{-1}$ ) (light blue line); (c) photosynthetic capacity ( $Pc$ ;  $gC\ m^{-2}\ d^{-1}$ ) (black line) and the ratio of  $GEP$  over  $PAR$  (black line), the light use efficiency ( $LUE$ ;  $gC\ MJ^{-1}$ ) (light blue line). At the bottom two panels, satellite derived data of: (d) MODIS Enhanced Vegetation Index at fixed solar zenith angle of  $30^\circ$  ( $EVI_{SZA30}$ ) (black line) and the Normalized Difference Vegetation Index ( $NDVI_{SZA30}$ ) (light blue line); (e) MODIS Leaf Area Index ( $LAI_{MOD}$ ) (black line) and MODIS Fraction of the Absorbed Photosynthetic Active Radiation ( $fPAR_{MOD}$ ) (light blue line). Grey boxes indicate Southern Hemisphere spring and summer (September to March). Black dashed vertical line indicates the timing of maximum  $GEP$ .



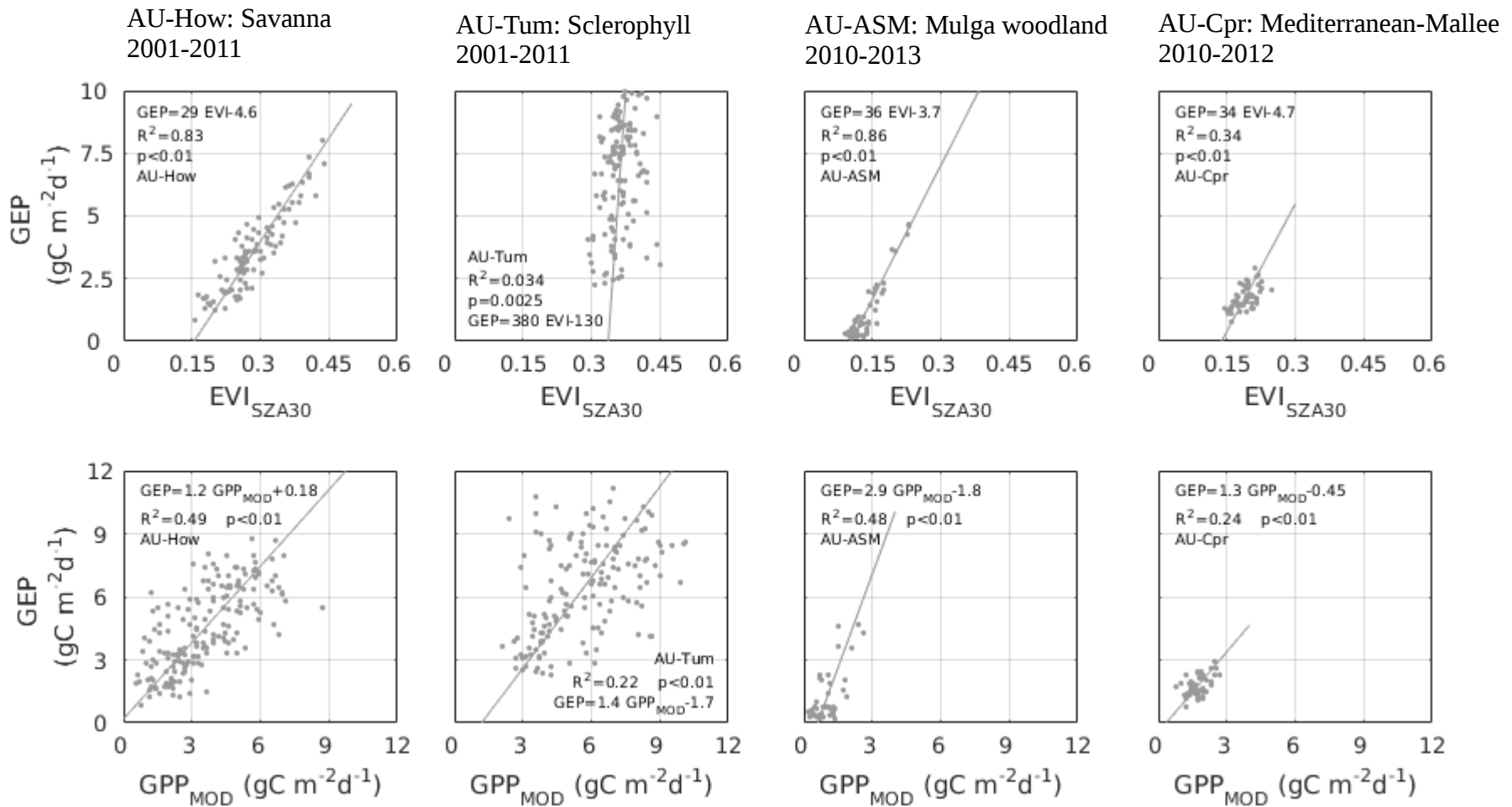


**Figure 5.** Top row: Linear regression between 16 and 8-day time series of measured gross ecosystem productivity ( $GEP$ ;  $\text{gC m}^{-2} \text{d}^{-1}$ ) (top row) and the MODIS fixed solar zenith angle of  $30^\circ$  enhanced vegetation index ( $EVI_{SZA30}$ ) at (a) Howard Springs (AU-How) open woodland savanna, (b) Alice Springs Mulga (AU-ASM), (c) Tumbarumba (AU-Tum) wet sclerophyll forest eddy, and (d) Chowilla Mallee (AU-Cpr) covariance site. Lower row: Regression between  $GEP$  and MODIS gross primary productivity ( $GPP_{MOD}$ ) (e) AU-How, (f) AU-Tum, (g) AU-ASM, and (h) AU-Cpr.

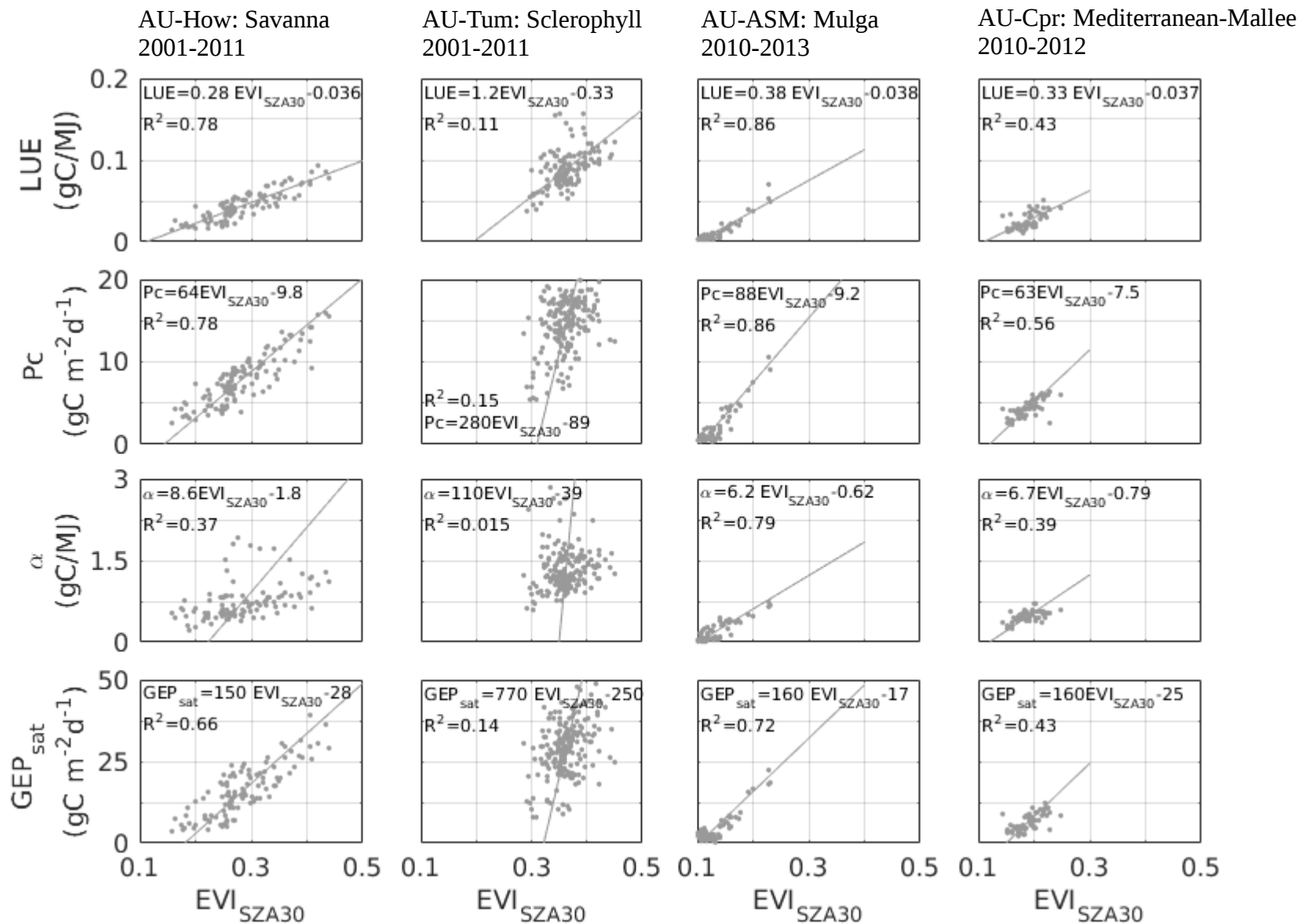


**Figure 6.** Relationships between 16-day mean values of (a) light use efficiency ( $LUE$ ;  $gC MJ^{-1}$ ), (b) photosynthetic capacity ( $Pc$ ;  $gC m^{-2} d^{-1}$ ), (c) ecosystem quantum yield ( $\alpha$ ;  $gC MJ^{-1}$ ), and (d)  $GEP$  at saturation light ( $GEP_{sat}$ ;  $gC m^{-2} d^{-1}$ ), and MODIS fixed solar zenith angle of  $30^\circ$  enhanced vegetation index ( $EVI_{SZA30}$ ). Four key Australian ecosystem sites, from left to right (columns), AU-How savanna, AU-ASM Mulga, wet sclerophyll forest of AU-Tum and AU-Cpr Mallee.

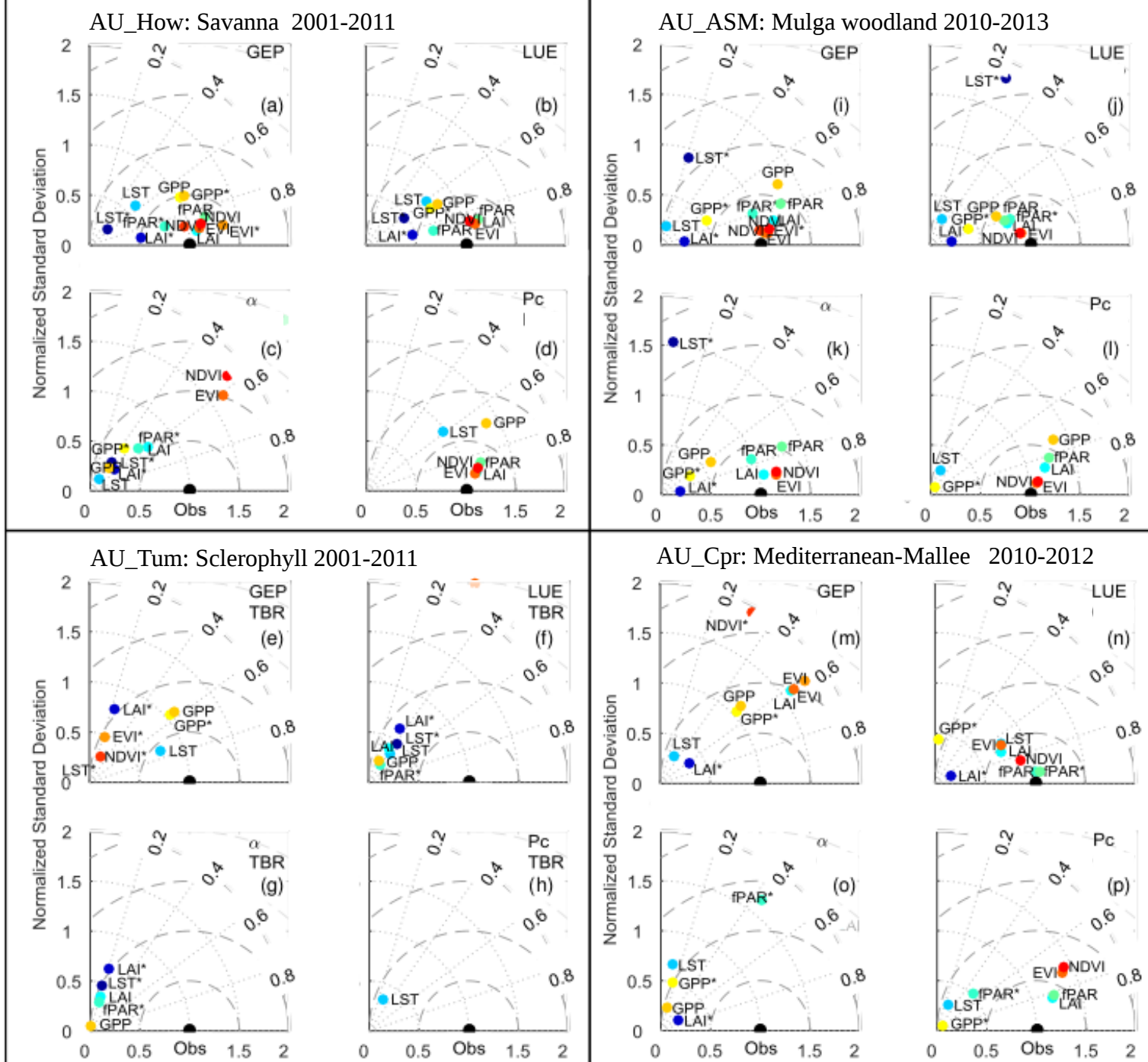


**Figure 7.** Taylor diagrams showing model results for Howard Springs (AU-How), Tumberumba (AU-Tum), Alice Springs (AU-ASM) and Calperum-Chowilla (AU-Cpr) based on site-specific and all sites linear regressions between gross ecosystem productivity (*GEP*), light use efficiency (*LUE*), photosynthetic capacity (*Pc*) and ecosystem quantum yield ( $\alpha$ ) and different remote sensing products MODIS fixed solar zenith angle of 30° Enhanced Vegetation Index (*EVI*) and Normalized Difference Vegetation Index (*NDVI*), Gross Primary Productivity product (*GPP*), daytime Land surface Temperature (*LST*), Leaf Area Index (*LAI*), fraction of the absorbed Photosynthetic Active Radiation (*fPAR*). All site relationships is labelled with an asterisk (e.g. *EVI\**). *EVI* and *NDVI* labels are used instead of *EVI*<sub>SZA30</sub> and *NDVI*<sub>SZA30</sub> for displaying purposes. Missing sites indicate that the model overestimates the seasonality of observations -model normalized standard deviation is >2.

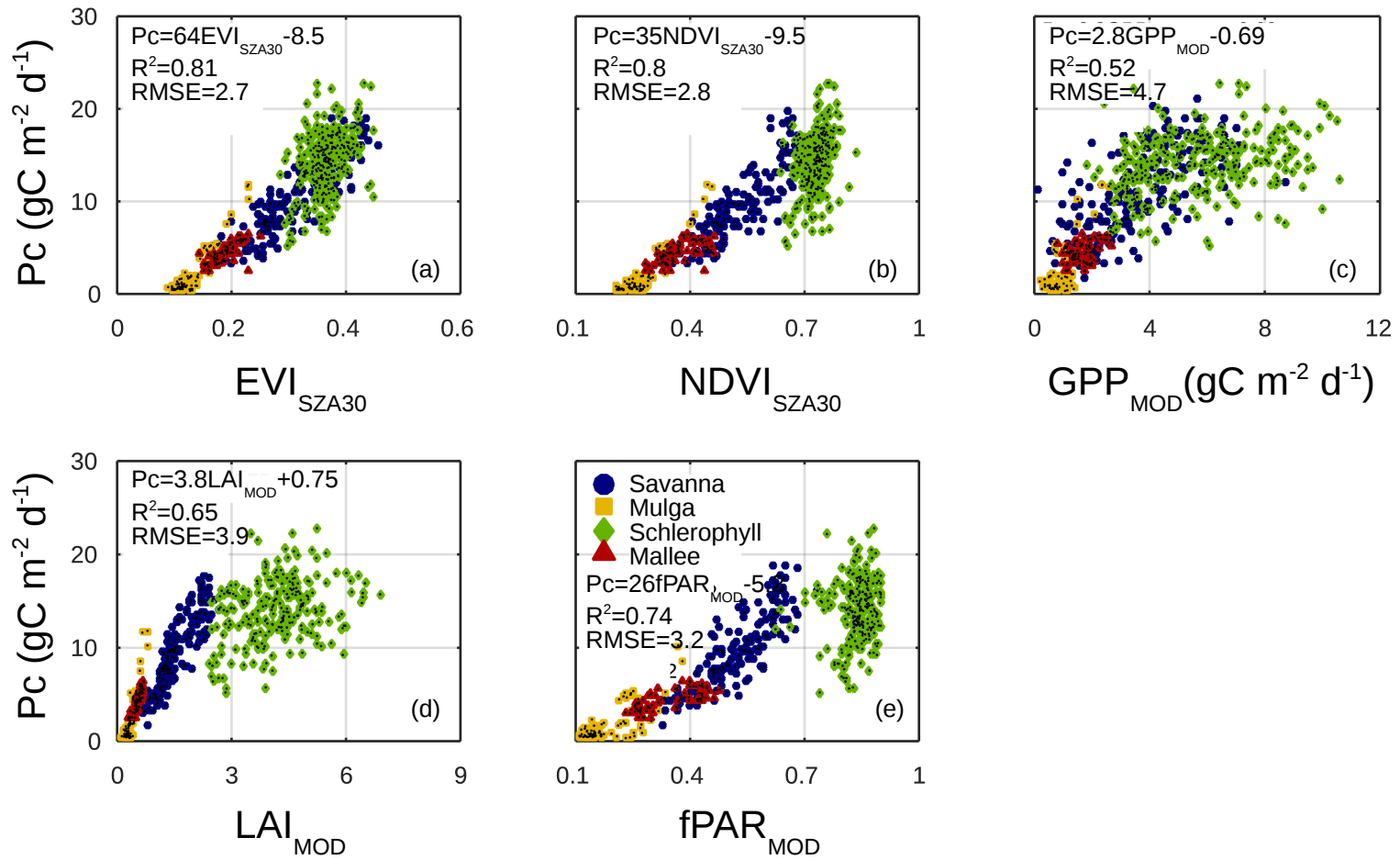


**Figure 8.** Relationships between 16-day mean values of photosynthetic capacity ( $P_c$ ;  $\text{gC m}^{-2} \text{d}^{-1}$ ) and different RS products: (a) MODIS fixed solar zenith angle of  $30^\circ$  enhanced vegetation index ( $\text{EVI}_{\text{SZA30}}$ ), (b) normalized difference vegetation index ( $\text{NDVI}_{\text{SZA30}}$ ), (c) MODIS gross primary productivity ( $\text{GPP}_{\text{MOD}}$ ;  $\text{gC m}^{-2} \text{d}^{-1}$ ), (d) leaf area index ( $\text{LAI}_{\text{MOD}}$ ), and (e) fraction of the absorbed photosynthetic active radiation ( $f\text{PAR}_{\text{MOD}}$ ). Four key Australian ecosystem sites included on the analysis: AU-How savanna (blue circles), AU-ASM Mulga (yellow square markers), AU-Cpr Mallee (red triangles) and wet sclerophyll forest of AU-Tum (green diamonds).

ID	Name	Measurement Period		Elevation (m.a.s.l.)	Lat/Lon (deg)		Vegetation Height (m)	Biome	u*tresh (m s <sup>-1</sup> )	u*min (m s <sup>-1</sup> )	u*max (m s <sup>-1</sup> )
		Start	End								
AU_How	Howard Springs	2001	2015	64	-12.50	131.15	15	Open woodland savanna	0.122	0.000	0.253
AU_ASM	Alice Springs Mulga	2010	2013	606	-22.28	133.25	6	Mulga	0.105	0.000	0.215
AU_Tum	Tumbarumba	2001	2014	1200	-35.66	148.15	40	Wet sclerophyll forest	0.173	0.000	0.421
AU_Cpr	Calperum-Chowilla	2010	2012	379	-34.00	140.59	5	Malle	0.176	0.086	0.265

**Table 1.** OZflux sites presented in this study -location and additional information.

<b>Product</b>	<b>Description</b>	<b>Data Source</b>	<b>Cell Size</b>	<b>Sample Size</b>	<b>Interval</b>
$LAI_{MOD}$	Leaf Area Index	MOD15A2	1000 m	1x1	8 Day
$fPAR_{MOD}$	Fraction of Absorbed PAR	MOD15A2	1000 m	1x1	8 Day
$LST_{day}$	Daytime Land Surface Temperature	MOD11A2	1000 m	1x1	8 Day
$GPP_{MOD}$	Gross Primary Production	MOD17A2	1000 m	1x1	8 Day
$EVI_{SZA30}$	NBAR Enhanced Vegetation Index	MCD43A1	500 m	2x2	8 Day
$NDVI_{SZA30}$	NBAR Normalied Difference Vegetation Index	MCD43A1	500 m	2x2	8 Day
$TRMM$	Mean Monthly Precipitation	TRMM	0.25 degree	1x1	Monthly
$SW_{CERES}$	Short wave radiation	CERES	1 degree	1x1	Monthly

**Table 2.** Remote sensing data sources, cell size, sample size (eddy-covariance tower-site at the center pixel) and time interval.

	AU_How				AU_ASM				AU_Tum				AU_Cpr				All			
	Coeff [a b c d]	CI	R <sup>2</sup>	AIC	Coeff	CI	R <sup>2</sup>	AIC	Coeff	CI	R <sup>2</sup>	AIC	Coeff	CI	R <sup>2</sup>	AIC	Coeff	CI	R <sup>2</sup>	AIC
GEP = a EVI + b	[21.94 -2.65]	[0.96 0.28]	0.82	263	[26.01 -2.48]	[1.69 0.2]	0.85	64	[15.52 0.90]	[5.55 2.01]	0.03	740	[12.74 -0.71]	[2.05 0.38]	0.36	49	[22.47 -2.19]	[0.51 0.1]	0.69	1323
GEP = a NDVI	[15.03 -4.11]	[0.70 0.35]	0.78	275	[14.34 -3.10]	[0.99 0.26]	0.83	80	[19.05 -7.28]	[5.23 3.79]	0.07	733	[3.97 0.24]	[1.29 0.46]	0.09	70	[12.62 -2.74]	[0.27 0.12]	0.72	1276
GEP = a LST <sub>day</sub> + b	[-0.22 70.91]	[0.02 7.70]	0.28	676	[-0.02 7.59]	[0.013 3.90]	0.03	218	<b>[0.26 -68.09]</b>	<b>[0.015 4.45]</b>	<b>0.58</b>	<b>656</b>	[0.017 -3.27]	[0.006 1.74]	0.12	69	[-0.095 32.57]	[0.01 3.13]	0.14	2279
GEP = a Precip <sub>TRMM</sub> + b	[0.01 3.03]	[0.001 0.11]	0.53	627	[0.01 0.38]	[0.004 0.11]	0.30	182	[-0.017 7.54]	[0.005 0.31]	0.03	799	[0.0006 1.66]	[0.003 0.097]	0.02	73	[0.009 3.60]	[0.001 0.14]	0.13	2340
GEP = a SW <sub>CERES</sub> + b	[-0.012 7.30]	[0.006 1.48]	0.02	781	[0.005 -0.30]	[0.002 0.59]	0.02	209	[0.026 1.025]	[0.001 0.26]	0.60	635	[0.003 1.14]	[0.0008 0.14]	0.12	67	[0.007 2.81]	[0.0016 0.32]	0.01	2329
GEP = a EVI + b LST <sub>day</sub> + c LST <sub>day</sub> EVI + d	[-29.96 127.38 0.09 -0.34]	[18.42 66.60 0.06 0.22]	0.82	268	[-11.51 76.94 0.03 -0.16]	[7.81 67.35 0.03 0.22]	0.87	66	[-2.64 1.38 0.08]	[0.21 10.71 0.04]	0.64	583	<b>[22.6 -145.8 -0.08 0.53]</b>	<b>[9.4 51.44 0.03 0.17]</b>	<b>0.63</b>	<b>30</b>	[-5.60 17.51 0.01 0.02]	[2.98 13.87 0.01 0.05]	0.70	1322
GEP = a EVI + b SW <sub>CERES</sub> + c SW <sub>CERES</sub> EVI + d	<b>[-3.57 24.15 0.003 -0.004]</b>	<b>[3.45 11.26 0.01 0.05]</b>	<b>0.82</b>	<b>266</b>	[2.48 -21.70 -0.02 0.19]	[0.99 8.68 0.004 0.03]	0.87	54	<b>[7.75 -19.41 -0.05 0.21]</b>	<b>[3.25 8.84 0.017 0.05]</b>	<b>0.70</b>	<b>553</b>	<b>[1.87 -4.52 -0.01 0.095]</b>	<b>[0.83 4.41 0.005 0.025]</b>	<b>0.62</b>	<b>26</b>	<b>[-0.31 4.95 -0.009 0.079]</b>	<b>[0.35 1.45 0.001 0.007]</b>	<b>0.82</b>	<b>1154</b>
GEP = a SW <sub>CERES</sub> + b SW <sub>CERES</sub> EVI + c	[3.63 -0.03 0.097]	[0.73 0.003 0.004]	0.82	263	<b>[-0.008 -0.01 0.10]</b>	<b>[0.18 0.001 0.006]</b>	<b>0.88</b>	<b>56</b>	[0.69 -0.014 0.12]	[0.29 0.006 0.016]	0.69	554	<b>[1.023 -0.01 0.07]</b>	<b>[0.097 0.001 0.008]</b>	<b>0.62</b>	<b>23</b>	[0.92 -0.014 0.1]	[0.13 0.001 0.002]	0.82	1179
GEP = a EVI + b Precip <sub>TRMM</sub> + c Precip <sub>TRMM</sub> EVI + d	<b>[-2.13 18.93 0.01 -0.02]</b>	<b>[0.34 1.28 0.004 0.01]</b>	<b>0.84</b>	<b>253</b>	<b>[-1.32 15.09 -0.019 0.18]</b>	<b>[0.25 2.19 0.005 0.04]</b>	<b>0.88</b>	<b>42</b>	[1.63 15.31 0.002 -0.04]	[3.78 10.29 0.06 0.16]	0.04	732	[0.21 6.96 -0.03 0.2]	[0.69 3.57 0.015 0.08]	0.52	43	[-2.35 22.48 0.008 -0.02]	[0.14 0.64 0.003 0.009]	0.66	1312
GEP = a NDVI + b LST <sub>day</sub> + c LST <sub>day</sub> EVI + d	[-57.78 118 0.17 -0.33]	[23.79 48.54 0.08 0.16]	0.79	279	[-24.42 79.28 0.07 -0.21]	[9.19 36 0.03 0.12]	0.86	75	[231 -416.25 -0.83 1.51]	[105.9 145.1 0.37 0.50]	0.68	566	<b>[34.5 -119.1 -0.12 0.43]</b>	<b>[10.8 29.76 0.036 0.1]</b>	<b>0.60</b>	<b>34</b>	[0.43 -27.31 -0.01 0.14]	[3.17 7.05 0.01 0.024]	0.79	1226
GEP = a NDVI + b SW <sub>CERES</sub> + c SW <sub>CERES</sub> NDVI + d	[-9.6 23.6 0.02 -0.03]	[4.76 9.06 0.02 0.04]	0.79	277	[2.77 -11.51 -0.02 0.10]	[1.38 5.41 0.006 0.02]	0.87	62	<b>[13.58 -17.68 -0.12 0.198]</b>	<b>[6.53 8.95 0.032 0.04]</b>	<b>0.71</b>	<b>542</b>	<b>[2.74 -5.59 -0.02 0.07]</b>	<b>[0.88 2.32 0.005 0.014]</b>	<b>0.60</b>	<b>30</b>	<b>[-0.75 2.8 -0.01 0.05]</b>	<b>[0.37 0.75 0.001 0.003]</b>	<b>0.88</b>	<b>1013</b>
GEP = a SW <sub>CERES</sub> + b SW <sub>CERES</sub> NDVI + c	[2.63 -0.031 0.07]	[0.79 0.004 0.003]	0.78	277	[-0.15 -0.01 0.06]	[0.19 0.001 0.004]	0.88	64	<b>[0.72 -0.056 0.11]</b>	<b>[0.29 0.01 0.014]</b>	<b>0.71</b>	<b>542</b>	[0.69 -0.01 0.04]	[0.12 0.002 0.005]	0.57	30	[0.64 -0.016 0.058]	[0.12 0.0006 0.001]	0.87	1052

**Table 3.** Linear regressions obtained by a non-linear mixed-effects regression model for gross ecosystem productivity ( $GEP$ ,  $\text{gC m}^{-2} \text{d}^{-1}$ ) versus combinations of 16-day average MODIS products: fixed solar zenith angle of  $30^\circ$  enhanced vegetation index ( $EVI_{\text{SZA}30}$ ), daytime and land surface temperature ( $LST_{\text{day}}$ ,  $^\circ\text{C}$ ), fixed solar zenith angle of  $30^\circ$  normalized difference vegetation index ( $NDVI_{\text{SZA}30}$ ), precipitation from the Tropical Rainfall Measuring Mission ( $Precip_{\text{TRMM}}$ ,  $\text{mm month}^{-1}$ ) data product from 1998-2013 (NASA, 2014b), and surface shortwave incident radiation from the Clouds and the Earth's Radiant Energy System ( $SW_{\text{CERES}}$ ,  $\text{W m}^{-2}$ ) data product from 2000–2013 (NASA, 2014a). Model runs for AU-How: Howard Springs, AU-ASM: Alice Springs Mulga, AU-Cpr: Calperum-Chowilla, and AU-Tum: Tumbarumba, and all available data (includes all sites). Bold fonts highlight values mentioned on the text.